A predictive viscosity model for aqueous electrolytes and organic–inorganic mixtures common to atmospheric aerosols

Joseph Lilek

Department of Atmospheric and Oceanic Sciences

McGill University, Montreal

July 2021

A thesis submitted to McGill University in partial fulfillment of the requirements of the degree of

Master of Science

Acknowledgements

I would like to express my gratitude to:

- My supervisor, Prof. Andreas Zuend, for his invaluable support throughout this project.
- My research group, whom I have gotten to know over a year of weekly Teams calls.
- Prof. Thomas Preston, for his review of this thesis.
- My mentor, Rex Buchanan, for great advice and edits over the years.
- My partner, Juliette Lavoie, for her patience, love, and support.
- The MOCCIE indoor chemistry modeling group, the Alfred P. Sloan Foundation, and Environment and Climate Change Canada for funding my research.

Abstract

Motivated by observations of viscous aerosols and their implications for the atmosphere, we have extended the thermodynamics-based group-contribution model AIOMFAC-VISC to predict viscosity for aqueous electrolyte solutions and aqueous organic–inorganic mixtures under realistic atmospheric conditions. First, we review existing viscosity models and measurement techniques, including newer droplet-based methods. For aqueous electrolyte solutions, our semi-empirical approach uses a physical expression based on Eyring's absolute rate theory, and we define activation energy for viscous flow as a function of temperature, ion activities, and ionic strength. For organic–inorganic mixtures, multiple mixing models were designed and tested to couple the AIOMFAC-VISC electrolyte model with its existing aqueous organic model. Adjustable parameters for ions and cation–anion pairs were simultaneously fitted to more than 6,000 data points covering concentrations from dilute to high ionic strength and temperatures between 263 and 333 K. The electrolyte model is shown to be highly accurate and capable of viscosity predictions for aqueous mixtures containing an arbitrary number of cation and anion species, including mixtures that have never been experimentally studied. Moreover, it provides physically meaningful extrapolations to extremely high electrolyte concentrations, which is essential in the context of microscopic aqueous atmospheric aerosols. We then present the best performing organic–inorganic mixing approaches implemented in AIOMFAC-VISC for reproducing viscosity measurements of aerosol surrogate systems.

Finally, AIOMFAC-VISC is discussed in the context of future work on aerosol modelling for diffusivity, phase separation, and gel transitions.

Abrégé

Motivés par les observations d'aérosols visqueux et leurs implications pour l'atmosphère, nous avons étendu le modèle de contribution de groupe AIOMFAC-VISC basé sur la thermodynamique pour prédire la viscosité des solutions électrolytiques aqueuses et des mélanges organiques–inorganiques aqueux dans des conditions atmosphériques réalistes. Tout d'abord, nous passons en revue les modèles de viscosité existants et les techniques de mesure, y compris les méthodes plus récentes basées sur les gouttelettes. Pour les solutions aqueuses d'électrolytes, notre approche semi-empirique utilise une expression physique basée sur la théorie du taux absolu de Eyring, et nous définissons l'énergie d'activation pour l'écoulement visqueux en fonction de la température, des activités ioniques et de la force ionique. Pour les mélanges organiques–inorganiques, plusieurs modèles de mélange ont été conçus et testés pour coupler le modèle d'électrolyte AIOMFAC-VISC avec son modèle organique aqueux existant. Des paramètres ajustables pour les ions et les paires cation-anion ont été simultanément ajustés à plus de 6 000 points de données couvrant des concentrations allant de la force ionique diluée à la force ionique élevée et des températures comprises entre 263 et 333 K. Le modèle d'électrolyte s'est révélé très précis et capable de prédire la viscosité de mélanges aqueux contenant un nombre arbitraire d'espèces de cations et d'anions, y compris des mélanges qui n'ont jamais été étudiés expérimentalement. De plus, il fournit des extrapolations physiquement significatives jusqu'à des concentrations d'électrolytes extrêmement élevées, ce qui est essentiel dans le contexte des aérosols atmosphériques aqueux microscopiques. Nous présentons en-

suite les approches de mélange organique–inorganique les plus performantes mises en œuvre dans AIOMFAC-VISC pour reproduire les mesures de viscosité des systèmes de substitution des aérosols. Enfin, AIOMFAC-VISC est discuté dans le contexte de travaux futurs sur la modélisation des aérosols pour la diffusivité, la séparation de phase et les transitions de gel.

Thesis Structure and Author Contributions

This thesis includes a brief research background, a manuscript, and recommendations for future work. The manuscript, which comprises Chapter 2, constitutes an original contribution to the field of atmospheric chemistry and will be submitted to the journal, Atmospheric Chemistry and Physics (ACP). Chapter 1 outlines the motivation for this work and Section 2.2 is the introduction of the manuscript. Both serve as a literature review for the thesis. All references for Chapter 2 are included in the reference list at the end of the thesis. Sections 2.3, 2.4, 2.5, and 2.7 are the main body of the research. Sections 2.3 and 2.4 outline the theory and methodology used to implement two upgrades to the AIOMFAC-VISC model: (1) a novel aqueous electrolyte viscosity model and (2) three approaches to predict the viscosity of aqueous organic–inorganic mixtures. Section 2.5 presents the main results of the aqueous electrolyte model and the organic–inorganic mixing models along with a discussion of the model performance. Section 2.7 functions as an appendix for the manuscript. Section 2.6 provides a summary of the work done in the manuscript. Finally, Chapter 3 discusses the utility of the AIOMFAC-VISC model and suggests areas for future work.

I carried out the research for this thesis: I researched existing viscosity models, gathered data from available literature, developed an original model, and assiduously tested and refined it. The original research framework was designed by Prof. Andreas Zuend

and he provided guidance throughout. I wrote all chapters of this thesis with editorial guidance from Prof. Andreas Zuend. During the preparation of this thesis, I was also co-author of a peer-reviewed article, Song et al. (2021), which was recently accepted for publication. My contribution to Song et al. (2021) was based on work presented in this thesis.

Contents

Chapter 1

Background

1.1 Overview and motivation

Atmospheric aerosols are tiny but important drivers of air chemistry, affecting weather, climate, and human health. They can be of different shapes and sizes, natural or human-made, organic or inorganic, or contain a mixture of both organic compounds and inorganic materials, including dissolved ions in aqueous solutions (Zhang et al., 2007; Hallquist et al., 2009; Fu et al., 2012). Aerosols range in diameter from a few nanometers (nm) to tens of micrometers ($\mu\mathrm{m}$), and their sizes and compositions affect their ability to scatter light (e.g. Pilinis et al., 1995; Rafferty and Preston, 2018), nucleate cloud droplets and ice particles (e.g. Yau and Rogers, 1996; Tan et al., 2014), and transport contaminants (e.g. Ariya et al., 2015; Kohanski et al., 2020).

Recent observations and laboratory measurements have demonstrated that aerosols (specifically their condensed phases) can exist in a variety of phase states with vastly different viscosities (Zobrist et al., 2008; Virtanen et al., 2010; Rovelli et al., 2019; Song et al., 2021). Viscosity, or more precisely dynamic viscosity, is a property of liquids that describes resistance to flow or deformation, and it can be grouped into three broad cat-

egories, for example as defined by Koop et al. (2011): liquid ($< 10^2$ Pa s), semi-solid (10^2 Pa s – 10^{12} Pa s), and amorphous solid or glassy ($> 10^{12}$ Pa s). Aerosol viscosity is a function of particle composition and temperature with a key influence from relative humidity (RH) related aerosol water uptake, due to the plasticizing effect of water. Aqueous organic aerosol phases often reach higher viscosity than aqueous electrolyte solutions under the same ambient conditions. Organic mixture viscosity can be calculated to first order as a combination of the pure-component viscosities (Irving, 1977; Viswanath et al., 2007), whereas aqueous electrolyte solutions include dissolved ions and cation–anion pairs within a solvent (water), necessitating a different modelling approach. Several inorganic species are commonly found in aerosols. Sea spray and dust emissions are the main source for nonvolatile ions (e.g., Na^+,K^+,Li^+,Mg^{2+},Ca^{2+}), while other ions like NH_4^+, NO_3^-, SO_4^{2-}, and halides can also originate from gas–particle partitioning and ion exchange processes of soluble gases (e.g. ammonia and nitric acid uptake in exchange for loss of HCl) with existing aerosols (Seinfeld and Pandis, 2016). Moreover, the size and electric charge of ions have been observed to affect their interaction with water molecules. Small, charge-dense ions and/or divalent ions like Na^+, Li^+, Mg^{2+}, Ca^{2+}, and SO_4^{2-} can bond more tightly to neighboring water molecules. These species have been identified as "structure-making," while large monovalent ions are termed "structure-breaking," referring to how they perturb the dynamic hydrogen-bond network of liquid water (Marcus, 2009).

Viscosity models have existed for over a century, but have only recently been applied or developed with aerosol particles in mind. For viscosity of organic aerosol mixtures, a combination of the Vogel–Tammann–Fulcher equation (DeRieux et al., 2018; Rothfuss and Petters, 2017) and the Gordon–Taylor mixing rule (Koop et al., 2011; Rothfuss and Petters, 2017) is a popular approach, but this requires measurements or estimates of the calorimetric glass transition temperature for each pure component in the mixture, which are rarely available for aqueous electrolyte solutions. While the viscosity of aqueous organic mixtures has been successfully modelled for aerosol particles (Gervasi et al., 2020),

a comprehensive, predictive model for the viscosity of aqueous organic–inorganic mixtures for aerosol particles has not yet been developed to our knowledge, and is presented in this thesis.

1.2 Measurement techniques for viscosity of aqueous electrolyte solutions and aqueous organic–inorganic mixtures

Although the focus of this thesis is on the development of molecular viscosity models for aerosol applications, it is prudent to describe the techniques used to measure viscosity of aqueous electrolyte solutions and organic–inorganic mixtures. Viscosity measurements have been collected for many aqueous electrolyte solutions at a wide range of concentrations and temperatures. Most of these are classified as "bulk measurements," i.e., with respect to a macroscopic bulk liquid as opposed to a discrete droplet or particle and using conventional viscometry or rheometry. Since the viscosities of aqueous electrolyte solutions tend to be low (for subsaturated solutions), these techniques are generally sufficient to measure viscosity of aqueous electrolyte solutions up to high ionic strength. For solids (e.g. crystallized solute), other metrics from rheology, like rigidity and viscoelastic properties are important to consider, but these are outside the scope of this thesis.

The challenge presented by aerosol size, the difficulty of measuring extremely high viscosities, and the interest in RH-induced phase changes have led to the invention of several new techniques to measure aerosol viscosity (Reid et al., 2018). Whereas bulk instruments such as commercial viscometers and rheometers measure viscosity of macroscopic material samples at known solute concentrations, the new, droplet-based techniques typically record how viscosity changes with RH and are therefore conducted under controlled RH conditions, with time allowed for the particles to equilibrate with the surrounding

air. To compare data from aerosol viscosity techniques with bulk measurements, particle water content or water activity can be predicted using a thermodynamic model, such as AIOMFAC (Aerosol Inorganic–Organic Mixtures Functional groups Activity Coefficients) (Zuend et al., 2008, 2011). This model will be discussed further in Chapter 2.

Two unique droplet-based techniques were first described by Renbaum-Wolff et al. (2013) to characterize the viscosity of α-pinene secondary organic aerosol, and they have since been used to measure viscosity of aqueous electrolyte solutions and aqueous organic–inorganic mixtures. The bead mobility method involves placing a droplet of the sample liquid on a hydrophobic substrate and incorporating $1\ \mu\mathrm{m}$ diameter melamine beads into the droplet. Sterilized $\mathrm{N_2}$ gas flows above the droplet, generating a shear stress that causes the sample liquid, including the beads, to circulate inside the droplet. Under a microscope, the movement of these beads within the droplet can be observed and the mean bead speed is used to calculate viscosity. This technique can measure viscosities between 10^{-3} and $10^{3}\ \mathrm{Pa\,s}$. The poke-flow method similarly involves depositing a droplet of sample liquid on a hydrophobic substrate, poking it with a high precision needle to form an indentation, and observing the time it takes for the droplet to relax back to its original shape (or some other relevant timescale, such as the e-folding time of the indentation diameter). This technique can probe viscosities above $10^{3}\ \mathrm{Pa\,s}$. In recent work, Song et al. (2021) used both the bead mobility and poke-flow techniques for measurements of the RH-dependent viscosity of aqueous $\mathrm{Ca(NO_3)_2}$ and $\mathrm{Mg(NO_3)_2}$, and aqueous mixtures of the two salts with sucrose.

Holographic optical tweezers, which use lasers to optically trap and levitate individual particles without the need for a substrate, have been used to measure aerosol viscosity, as well as microrheology and diffusion of water (Power et al., 2013; Davies and Wilson, 2016). For example, the coalescence timescale of two micron-sized suspended droplets was used to determine viscosity of aqueous $\mathrm{NaNO_3}$ and aqueous mixtures of $\mathrm{NaNO_3}$ with sucrose (Baldelli et al., 2016; Rovelli et al., 2019). This technique is expected to capture

viscosities between 10^{-3} and 10^{9} $\mathrm{Pa\,s}$. The actual droplet composition at set RH cannot be directly measured, only inferred from thermodynamic models, adding uncertainty. Similar to the optical tweezers approach, the dual-balance linear quadrupole electrodynamic balance technique developed by Richards et al. (2020a) does not require a substrate, and it has been used to study ion–organic interactions and gel transitions in aqueous organic–inorganic mixtures containing divalent ions (Richards et al., 2020b).

In particle rebound measurements, a solution is prepared, nebulized, and sent through a chamber to collide with an impactor plate. The fraction of rebounding versus adhering or splashing particles is calculated across the RH range, and this rebound fraction is used as a proxy variable to indicate high viscosity in those particles, while the splashing or adhering ones are seemingly liquid-like (Virtanen et al., 2010). This technique has been used to infer high viscosity or gel formation for aqueous inorganic aerosol (Li et al., 2017). Unlike the previous techniques, particle rebound studies have not been used to report viscosity measurement values. However, due to their relatively simple and robust design, they have been adopted for approximate aerosol viscosity measurements in field studies (Virtanen et al., 2010; Bateman et al., 2015, 2016).

1.3 Models for viscosity of aqueous electrolyte solutions

Many models exist for aqueous electrolyte viscosity, and here we describe several of the models that have been developed and used over the last century. These models can be roughly grouped into three categories: Jones–Dole-type models, Eyring-type models, and correlative models without a theoretical basis, e.g., system-specific polynomial fits.

Jones and Dole (1929) identified a relationship for relative fluidity of binary aqueous electrolyte solutions; the inverted form is called the Jones–Dole equation, which has the form

$$\eta_{\mathrm{rel}} = \frac{\eta_{\mathrm{exp}}}{\eta_0} = 1 + A\sqrt{c} + Bc. \tag{1.1}$$

Here η_{rel} is the relative (dynamic) viscosity, η_{exp} is the measured viscosity, η_0 is the pure component viscosity of the reference solvent, c is the molarity of the dissolved electrolyte, A is a constant that represents the long-range electrostatic forces between ions in solution, and B is the Jones–Dole coefficient (or sometimes simply called the B-coefficient), an empirical constant that defines the contribution from short-range ion–solvent interactions to the viscosity of the solution. A and B have been calculated for many systems, with different values for each electrolyte. Kaminsky (1957) added a third term (with an additional fit parameter), which allows the Jones–Dole equation to represent viscosity for slightly higher concentrations. Jenkins and Marcus (1995) aggregated ionic B-coefficients for aqueous and non-aqueous solutions of many electrolytes over a broad range of temperatures, based on a reference electrolyte assumption. Lencka et al. (1998) adapted the Jones–Dole equation for concentrated aqueous electrolyte mixtures, including a term based on ionic strength to capture the steep increase in viscosity at high concentrations. They also used a thermodynamic model to account for chemical speciation.

Another framework that has gained momentum is that of Glasstone, Eyring and co-authors, who outlined an equation based on absolute rate theory to describe viscosity (Glasstone et al., 1941). Unlike the Jones–Dole equation, their equation, which we refer to here as the Eyring equation, takes an exponential form reminiscent of the Arrhenius equation,

$$\eta = \frac{hN_{\mathrm{A}}}{V} e^{\Delta g^* / (RT)}. \tag{1.2}$$

Here, h is the Planck constant, N_{A} is Avogadro's constant, R is the universal gas constant and T is the solution temperature in K. V is the average molar volume of the liquid. The molar Gibbs energy of activation for viscous flow, Δg^* (units of $\mathrm{J\,mol^{-1}}$), is a non-measurable term that can be calculated for liquids for which the viscosity is known (assuming validity of Eq. 1.2). Goldsack and Franchetto (1977b) developed a model based on this framework that was fitted for aqueous solutions of several halide and sulfate salts, as well as ternary and quaternary mixtures. They also related their model to the Jones–Dole

coefficients, which were more recognized at the time. As tested by Nowlan et al. (1980), the Goldsack–Franchetto model was found to fail at higher concentrations with some electrolytes requiring multiple sets of parameters to accurately cover different concentration ranges. The model described by Esteves et al. (2001) combines theoretical frameworks from Eyring and Debye–Hückel theory and is fitted for 21 binary solutions of strong electrolytes in water, methanol, ethanol, and 1-butanol. Hu and Lee (2003) introduced a predictive model for mixtures of aqueous electrolyte solutions based on the Zdanovskii–Stokes–Robinson (ZSR) mixing rule (Zdanovskii, 1948, 1936; Stokes and Robinson, 1966) where two binary aqueous solutions are measured at the same water activity and then combined in such proportion that the resulting mixture is of the same water activity as the two original solutions, i.e., at isopiestic equilibrium.

Correlative models generally lack a physicochemical justification, but provide excellent agreement over the concentration range of available data. This category includes system-specific polynomial equations, which are not predictive. It also includes models with non-polynomial forms, such as the original empirical model for viscosity of aqueous electrolyte solutions developed by Laliberté (2007a).

Whereas early models were only useful for highly dilute solutions, more recent models capture non-ideal behavior and predict viscosity to much higher electrolyte concentrations. In developing the model presented in this work, inspiration was taken from several frameworks and ideas, which are further detailed in the next three sections.

1.3.1 Ionic contributions from B-coefficients

Viscosity B-coefficients for Jones–Dole type equations have been reported for various electrolytes in water and other solvents. Cox et al. (1934) first suggested that B-coefficients from Eq. (2.1) could be split into additive ionic contributions and Kaminsky (1957) and others have used this assumption in their work. These authors reasoned that some elec-

trolytes like KCl contain a cation and an anion of similar enough size and charge magnitude that they could be assumed to make equivalent contributions to viscosity. Therefore, the B-coefficient for KCl can be evenly split into contributions for $\mathrm{K^+}$ and $\mathrm{Cl^-}$ that both equal $\frac{1}{2}B_{\mathrm{KCl}}$. Through this approximation, in which KCl or another suitable salt acts as a reference electrolyte, ionic B-coefficients have been defined sequentially for many ions – first those paired with either $\mathrm{K^+}$ or $\mathrm{Cl^-}$ and then others – at a wide range of temperatures (Jenkins and Marcus, 1995). In theory, these can be added to calculate the viscosity of any multi-ion solution. In practice, however, the Jones–Dole equation is only reliable for electrolyte concentrations up to $0.1\ \mathrm{M}$, and the extension by Kaminsky only up to $\sim 0.3\ \mathrm{M}$ (Viswanath et al., 2007). The powerful idea that solution viscosity can be represented by contributions from individual dissolved ions as opposed to ions associated into neutral salt/electrolyte units is adapted for the model presented in this work and extended over a broad concentration range.

1.3.2 The Goldsack–Franchetto model

Goldsack and Franchetto (1977b) simplified the Eyring equation by defining the energy and volume parameters, E and V. They fitted their model parameters to viscosity measurements for binary aqueous electrolyte solutions up to moderate ($1 - 3\ \mathrm{molal}$) and high concentrations ($3 - 10\ \mathrm{molal}$). Their equation is

$$\eta = \frac{\eta_{\mathrm{w}}\, e^{XE}}{1 + XV}, \tag{1.3}$$

where X is the mole fraction of the dissociated cation or anion. For a 1:1 electrolyte, their expressions are

$$\eta_{\mathrm{w}} = \frac{hN_{\mathrm{A}}}{V_{\mathrm{w}}} e^{\Delta g^*_{\mathrm{w}}/(RT)}, \tag{1.4}$$

$$E = \frac{\Delta g^*_c + \Delta g^*_a - 2\Delta g^*_{\mathrm{w}}}{RT}, \tag{1.5}$$

$$V = \frac{V_c + V_a}{V_{\mathrm{w}}} - 2. \tag{1.6}$$

In the above expressions, the subscripts c, a, and w denote the cation, anion, and pure water, respectively, and $X = X_c$. Goldsack and Franchetto (1977a) showed that their equation could also accommodate asymmetric electrolytes and mixtures of more than one electrolyte. They initially reported E and V parameters for several halide salts, but values were later defined for sulfate and nitrate salts. The E and V parameters were fitted for temperatures between $0°\mathrm{C}$ and $60°\mathrm{C}$ at $5°\mathrm{C}$ increments (Goldsack and Franchetto, 1978). Nowlan et al. (1980) found that the Goldsack–Franchetto model failed for high concentrations of binary aqueous solutions of divalent salts like $\mathrm{Ca(NO_3)_2}$ and $\mathrm{MgSO_4}$. The Goldsack–Franchetto model is the first example of an aqueous electrolyte viscosity model based on Eyring theory, which indicated the promise of this approach.

1.3.3 The Laliberté model

In 2007, Laliberté published a comprehensive viscosity model for aqueous electrolyte solutions. In developing his model, Laliberté eventually aggregated data for 95 different solutes and fit the data with an original exponential-form equation (Laliberté, 2007a,b, 2009). The viscosity behavior of each binary electrolyte solution is captured by six empirically determined coefficients. This model is one of the most accurate viscosity models published to date, but it lacks a rigorous physicochemical justification. Another drawback of Laliberté's model is spurious behavior at high concentrations for several electrolyte so-

lutions beyond the concentration range covered by experimental data, which he notes explicitly (Laliberté, 2007a). Laliberté also does not include a mechanism for splitting the total viscosity into ionic contributions, instead defining a hypothetical solute viscosity term, η_s, as

$$\eta_s = \frac{e^{[(\upsilon_{1,s}(1-w_{\mathrm{w}})^{\upsilon_{2,s}}+\upsilon_{3,s})/(\upsilon_{4,s}(T-273.15)+1)]}}{\upsilon_{5,s}(1-w_{\mathrm{w}})^{\upsilon_{6,s}}+1}, \tag{1.7}$$

where $\upsilon_{1,s}$ to $\upsilon_{6,s}$ denote the coefficients for solute s, w_{w} is the mass fraction of water, and T is the temperature in K. To calculate the solution viscosity, η_{mix}, Laliberté employs a mass-fraction-weighted mixing rule (geometric mean). This mixing rule also works to determine the viscosity of ternary or quaternary mixtures as follows:

$$\eta_{\mathrm{mix}} = \prod_k \eta_k^{w_k}. \tag{1.8}$$

Here k covers all mixture components (solutes and water), η_k is the viscosity of component k, and w_k is the mass fraction of component k. Laliberté's model correlates with measurements of binary aqueous electrolyte solutions up to high concentrations and has some predictive capacity for ternary and quaternary mixtures. Verifying the predictions for mixtures with $w_{\mathrm{w}} < 0.5$ is often challenging due to the lack of available measurements. Frequently, bulk solution measurements at $w_{\mathrm{w}} < 0.5$ are not possible due to the tendency for highly concentrated electrolyte solutions, approaching and exceeding salt solubility limits, to crystallize into salts (or salt hydrates) before liquid viscosity can be ascertained. In this context, it is worth noting that viscosity models typically ignore solute crystallization, instead producing smooth extrapolations throughout the concentration range covered.

1.4 Models for aqueous organic–inorganic mixtures

While many models exist for organic mixtures and aqueous electrolyte mixtures, very few models can accommodate aqueous organic–inorganic mixtures. Bajić et al. (2014) used the Eyring equation and thermodynamic modeling to predict the viscosity of mixtures of ionic liquids and organic solvents. Wang et al. (2004) extended the Lencka et al. (1998) model to accommodate aqueous organic–inorganic mixtures. The prior work in our research group by Gervasi et al. (2020) in developing AIOMFAC-VISC, made designing a new, thermodynamics-based aqueous electrolyte model and combining it with the existing organic mixture model the most attractive approach.

Chapter 2

A predictive viscosity model for aqueous electrolytes and mixed organic–inorganic aerosol phases

Joseph Lilek[1] and Andreas Zuend[1]

[1]Department of Atmospheric and Oceanic Sciences, McGill University, Montreal, Quebec, Canada

The following chapter is a manuscript to be submitted to the journal, Atmospheric Chemistry and Physics. JL performed the research, wrote the manuscript, and created the figures. AZ created the original research framework, provided research direction, and edited the manuscript.

2.1 Abstract

Aerosol viscosity is determined by mixture composition and temperature, with a key influence from relative humidity in modulating aerosol water content. Aerosol particles frequently contain mixtures of water, organic compounds and inorganic ions, so we have extended the thermodynamics-based group-contribution model AIOMFAC-VISC to predict viscosity for aqueous electrolyte solutions and aqueous organic–inorganic mixtures. For aqueous electrolyte solutions, our semi-empirical approach uses a physical expression based on Eyring's absolute rate theory, and we define activation energy for viscous flow as a function of temperature, ion activities, and ionic strength. The AIOMFAC-VISC electrolyte model's ion-specific expressions were simultaneously fitted, which arguably makes this approach more predictive than that of other models. This also enables viscosity calculations for aqueous solutions containing an arbitrary number of cation and anion species, including mixtures that have never been experimentally studied. These predictions achieve an excellent level of accuracy while also providing physically meaningful extrapolations to extremely high electrolyte concentrations, which is essential in the context of microscopic aqueous atmospheric aerosols. For organic–inorganic mixtures, multiple mixing approaches were tested to couple the AIOMFAC-VISC electrolyte model with its existing aqueous organic model. We discuss the best performing mixing models implemented in AIOMFAC-VISC for reproducing viscosity measurements of aerosol surrogate systems. Finally, we present advantages and drawbacks of different model design choices and associated computational costs of these methods, of importance for use of AIOMFAC-VISC in dynamic simulation.

2.2 Introduction

2.2.1 Viscosity and aerosols

The dynamic viscosity of various fluids and fluid mixtures is an important material property in industrial applications, cooking, and earth system science at large and small scales. The dynamic viscosity of a fluid characterizes its resistance to flow or deformation; its inverse is known as the fluidity. In the context of aerosol phases, viscosity is also important due to its relationship with the dynamics and timescales of molecular mixing and diffusion (Koop et al., 2011; Reid et al., 2018). At room temperature, liquid water has a dynamic viscosity of approximately $10^{-3}\ \mathrm{Pa\,s}$; honey one of approximately $10^{1}\ \mathrm{Pa\,s}$ and pitch approximately $10^{8}\ \mathrm{Pa\,s}$. One can intuitively understand viscosity when attempting to pour each of these fluids out of a container: Water and honey clearly move, albeit at different speeds, while pitch is imperceptibly slow. It is useful to separate the viscosity regimes encountered in aerosol particles and other amorphous solutions into three broad categories, for example as defined by Koop et al. (2011): liquid ($< 10^{2}\ \mathrm{Pa\,s}$), semi-solid ($10^{2}\ \mathrm{Pa\,s}$ – $10^{12}\ \mathrm{Pa\,s}$), and amorphous solid or glassy ($> 10^{12}\ \mathrm{Pa\,s}$).

Aerosols impact climate and public health. Natural and anthropogenic processes introduce immense quantities of primary and secondary aerosols into the atmosphere, including organic and elemental carbon, sulfates, nitrates, chlorides, and other inorganic material. Reactive organic compounds can form secondary organic aerosol (SOA), which can homogeneously nucleate or deposit onto preexisting aerosol (Hallquist et al., 2009; Heald and Kroll, 2020). Aerosol particles often contain a mixture of inorganic and organic matter (Zhang et al., 2007); this is especially true in urban environments (Fu et al., 2012). As relative humidity (RH) changes, organic–inorganic mixtures will uptake or release water, which changes the concentration of solutes such as inorganic electrolytes and can potentially induce liquid–liquid phase separation (Shiraiwa et al., 2013); in fact, the individual "liquid" phases could also be semi-solid or even glassy in terms of viscosity.

At very high RH (including water supersaturation), aerosol particles may uptake water to the point where they become or remain homogeneously mixed liquid-like solution droplets while at lower RH, phase separation can occur and one or more of these phases can become relatively viscous. Such RH-dependent viscosity transitions have been observed in laboratory experiments of surrogate aerosol mixtures and reproduced in modelling studies (Reid et al., 2018). That aerosols can be highly viscous under certain conditions has raised a number of interesting questions. Does a high viscosity in an aerosol phase significantly impact the rates of heterogeneous oxidation, multiphase chemistry, or ion-displacement reactions (Zhou et al., 2019; Fard et al., 2017)? How does viscosity affect the equilibrium timescale of gas–particle partitioning for semivolatile organic compounds (Shiraiwa and Seinfeld, 2012)? Does high viscosity substantially slow the rate of water uptake and release (Wallace and Preston, 2019)? And under what environmental conditions and for which chemical compositions do we observe a glassy aerosol state (Zobrist et al., 2008; Koop et al., 2011)? Predictive viscosity models that can accommodate the varied chemistry and non-ideal behavior of aerosol mixtures should allow us to quantify these effects.

2.2.2 Two popular frameworks: Jones–Dole and Eyring

The two main theoretical frameworks for viscosity of aqueous electrolyte solutions are the Jones–Dole and the Eyring equations. The Jones–Dole equation is one of the earliest identified relationships for relative viscosity and is expressed as

$$\eta_{\mathrm{rel}} = \frac{\eta_{\mathrm{exp}}}{\eta_0} = 1 + A\sqrt{c} + Bc, \tag{2.1}$$

where η_{rel} is the relative (dynamic) viscosity, η_{exp} is the measured viscosity, η_0 is the pure component viscosity of the reference solvent, c is the molarity of the dissolved electrolyte before dissociation, A is a semi-empirical constant that represents the long-range electro-

static forces between ions in solution described by Debye–Hückel theory, and B is the Jones–Dole coefficient (or sometimes simply called the B-coefficient), an empirical constant that defines the contribution from short-range ion–solvent interactions to the viscosity of the solution (Jones and Dole, 1929). A and B have been calculated for many electrolytes and at many temperatures, with values available in the literature. The original Jones–Dole equation is only useful for dilute electrolyte solutions, but later extensions added parameters and terms to extend the concentration range in which it is applicable (Kaminsky, 1957; Lencka et al., 1998; Wang et al., 2004). The use of a reference electrolyte assumption can also be used to solve for ionic B-coefficients. For example, KCl contains a cation and an anion of roughly the same size and charge magnitude. Therefore, the B-coefficient for KCl can be evenly split into contributions for $\mathrm{K^+}$ and $\mathrm{Cl^-}$ that both equal $\frac{1}{2}B_{\mathrm{KCl}}$ (Cox et al., 1934; Kaminsky, 1957). B-coefficents for many ions have been calculated using the same basic approach (Jenkins and Marcus, 1995).

Glasstone et al. (1941) introduced another equation for viscosity based on absolute rate theory, which we call the Eyring equation:

$$\eta = \frac{hN_{\mathrm{A}}}{V} e^{\Delta g^*/(RT)}. \tag{2.2}$$

Here, h is the Planck constant, N_{A} is Avogadro's constant, R is the universal gas constant and T is the solution temperature in K. V is the average molar volume of the solution. The molar Gibbs energy of activation for viscous flow, Δg^* (units of $\mathrm{J\,mol^{-1}}$), is a non-measurable term that can be calculated for liquids for which the viscosity is known or split into additive contributions. The Eyring equation has been tested extensively in earlier works (Goldsack and Franchetto, 1977a,b, 1978; Esteves et al., 2001; Hu and Lee, 2003; Bajić et al., 2014), and has been shown to accurately predict viscosity to higher concentrations than the Jones–Dole equation. The Eyring equation is therefore more attractive for fields that demand accurate viscosity predictions over the full range from highly dilute to highly concentrated aqueous solutions, such as applications in atmospheric aerosols.

2.2.3 Our model: AIOMFAC-VISC

AIOMFAC-VISC, the model applied and further extended in this study, was first introduced by Gervasi et al. (2020) as a thermodynamics-based model for predicting the viscosity of aqueous organic mixtures. In this work, we extend the AIOMFAC-VISC model for the prediction of the viscosity of aqueous electrolyte solutions, obtaining a level of accuracy close to that of the engineering-oriented empirical model developed by Laliberté (2007a), while using fewer parameters and a more physically-justifiable equation. Moreover, we enable AIOMFAC-VISC to predict viscosity for aqueous organic–inorganic mixtures applicable to aerosol phases across the the observed meteorological ranges of temperature, RH, and chemical composition. "AIOMFAC-VISC" refers to the full viscosity model, which comprises "the electrolyte model" and "the organic model." This distinction becomes especially important when considering aqueous organic–inorganic mixtures.

AIOMFAC-VISC is contained within the Aerosol Inorganic–Organic Mixtures Functional groups Activity Coefficients (AIOMFAC) model, a group-contribution thermodynamic model which explicitly describes the interaction of organic compounds, inorganic ions, and water (Zuend et al., 2008, 2011). AIOMFAC can be run for specific mixture compositions and temperatures as a standalone activity coefficient model or as part of an extended equilibrium framework to compute equilibrium gas–particle partitioning, including liquid–liquid phase separation predictions (Zuend et al., 2010; Zuend and Seinfeld, 2012; Pye et al., 2018, 2020). In the latter case, the fully developed AIOMFAC-VISC model, detailed in the next sections, allows for the prediction of viscosities in coexisting liquid, semi-solid, or amorphous solid phases containing water, organic compounds, and inorganic ions.

2.3 Theory

2.3.1 Applying Eyring's basis for aqueous electrolyte viscosity in AIOMFAC-VISC

Using a known value for the viscosity of pure water, η_{w}, Eq. (2.2) becomes

$$\Delta g_{\mathrm{w}}^{*} = RT \ln\left(\frac{\eta_{\mathrm{w}} V_{\mathrm{w}}}{h N_{\mathrm{A}}}\right), \tag{2.3}$$

where V_{w} and $\Delta g_{\mathrm{w}}^{*}$ are the average molar volume and average molar Gibbs energy of activation for viscous flow of pure water. In aqueous electrolyte solutions, knowing $\Delta g_{\mathrm{w}}^{*}$ and V_{w} allows us to solve algebraically for the Δg^{*} and V contributions of the dissolved ions. Goldsack and Franchetto (1977b) split these contributions as

$$\Delta g^{*} = x_{\mathrm{w}} \Delta g_{\mathrm{w}}^{*} + \sum_{i=1}^{J} x_i \Delta g_i^{*} \tag{2.4}$$

and

$$V = x_{\mathrm{w}} V_{\mathrm{w}} + \sum_{i=1}^{J} x_i V_i. \tag{2.5}$$

Here, J is the number of different kinds of ions in the mixture, x_i is the mole fraction of ion i defined on the basis of dissociated ions, and x_{w} is the mole fraction of water. Ionic Δg^{*} contributions can be calculated, as has been previously shown for B-coefficients (Goldsack and Franchetto, 1977b).

Equation (2.2) depends on the molar Gibbs energy of activation for viscous flow, a quantity that can be estimated but is not directly measurable. According to Eyring, viscosity can be conceptualized as the transient formation and refilling of holes in a fluid as molecules or ions diffuse through the fluid interior. This concept informs our model design. While Goldsack and Franchetto (1977b) used a modified form of the Eyring equation that emphasized binary and ternary mixtures, AIOMFAC-VISC accommodates an arbi-

trary number of cation and anion species in any proportion and with the added benefit of some level of predictability for aqueous electrolyte systems containing ions in combinations that have never been studied experimentally.

2.3.2 Deriving an expression for the molar Gibbs energy for viscous flow

Equation (2.2) provides an expression for mixture viscosity that depends on an effective average molar Gibbs energy of activation – see Eq. (2.4). Since the molar Gibbs energy of activation for viscous flow of a single ionic species, e.g. Na^{+}, cannot be measured and using the reference electrolyte assumption would introduce too much uncertainty, we turn to thermodynamic theory to define an equation to estimate it. First, consider the molar Gibbs energy contribution of an ionic species to a thermodynamic phase at constant temperature and pressure, $g_i = \mu_i$, where μ_i is the chemical potential of ion i. Analogously, we can introduce a molar Gibbs energy of activation for viscous flow, g_i^*. This activated-state energy can be compared to an inactivated reference state (representing equilibrium conditions), g_i^{ref}, such that Δg_i^* is defined as

$$\Delta g_i^* = g_i^* - g_i^{ref}, \tag{2.6}$$

or equivalently,

$$\Delta g_i^* = \mu_i^* - \mu_i^{ref}. \tag{2.7}$$

μ_i^* and μ_i^{ref} can be expressed as

$$\mu_i = \mu_i^{\circ,(m)}(p^\circ, T, m^\circ) + RT \ln [a_i^{(m)}], \tag{2.8}$$

where μ_i° is the standard-state chemical potential, and $RT \ln [a_i^{(m)}]$ is a correction term that depends on the ion activity, $a_i^{(m)}$, with superscript (m) denoting activity defined on

a molality basis. For ions it is common to use a molality basis, such that the ion activity, a_i, is defined as the molality of the ion, m_i, normalized by unit molality, $m^\circ = 1\ \mathrm{mol\,kg^{-1}}$, and multiplied by the activity coefficient of the ion, γ_i (e.g. Zuend et al., 2008):

$$a_i^{(m)} = \frac{m_i}{m^\circ}\gamma_i^{(m)}. \tag{2.9}$$

AIOMFAC defines ion molality as moles of dissociated ion per $1\ \mathrm{kg}$ of solvent mixture (water + organics) as opposed to per $1\ \mathrm{kg}$ of water, and this must be taken into account when organics are present. For the sake of simpler notation, we will hereafter omit superscript (m) as molality basis will consistently be used for all ions in this work. Equation (2.7) then becomes

$$\Delta g_i^* = \mu_i^{\circ,*} + RT\ln[a_i^*] - \mu_i^{\circ,ref} + RT\ln[a_i^{ref}]. \tag{2.10}$$

During viscous flow, the standard-state chemical potential does not change and we define $\mu_i^{\circ,*} = \mu_i^{\circ,ref}$. Therefore, Eq. (2.10) simplifies to

$$\Delta g_i^* = RT\ln[a_i^*] - RT\ln[a_i^{ref}], \tag{2.11}$$

or simpler still,

$$\frac{\Delta g_i^*}{RT} = \ln\left(\frac{a_i^*}{a_i^{ref}}\right). \tag{2.12}$$

The problem shifts from defining the molar Gibbs energy for viscous flow to quantifying the activation activity for viscous flow. It is assumed that this special activity a_i^* is a function of the reference activity, a_i^{ref}. Therefore, $a_i^* = f(a_i^{ref})$, which by Eq. (2.9) implies dependence on γ_i^{ref} and the molality, m_i. Thus, $\frac{\Delta g_i^*}{RT} = f(\gamma_i^{ref}, m_i)$.

2.3.3 Contributions to Gibbs energy for viscous flow

In our model, this energy is decomposed into three component-specific, additive contributions. First, the energy required for solvent molecules to move from their original locations into vacant holes, or to form new holes, is the molar Gibbs energy for viscous flow of the solvent, Δg^*_{w}. Here we focus on water as the only solvent of ions for the purpose of this part of the AIOMFAC-VISC model for aqueous electrolyte solutions; mixtures of water, organics, and ions will be considered in Section 2.4.4. Second, the energy required for dissolved ions to move from their original locations into vacant holes is the molar Gibbs energy for viscous flow of the ions, Δg^*_i. Third, in highly concentrated solutions, cations and anions can interact sufficiently frequently that they can impact the viscosity of the solution. The energy required for temporarily coupled cation–anion entities to move from their original locations into vacant holes is the molar Gibbs energy for viscous flow for cation–anion pairs, $\Delta g^*_{c,a}$. Finally, Eq. (2.3) is used to define the molar activation energy for viscous flow for water.

Gibbs energy contributions from ions and cation–anion pairs

Each individual ion is assigned two coefficients, $c_{0,i}$ and $c_{1,i}$, and we express $\frac{\Delta g^*_i}{RT}$ by the functional form

$$\frac{\Delta g^*_i}{RT} = c_{0,i} \ln \left(a_i^{ref}\right) + c_{1,i}. \tag{2.13}$$

Here, a_i^{ref} is considered to be the molal ion activity for the given mixture composition, e.g. computed with AIOMFAC. Initial tests indicated that the use of a single fit parameter per ion would provide inadequate flexibility for the model to fit experimental data, so a second parameter was included in Eq. (2.13). In our approach, we have no need for a reference electrolyte assumption, as molar Gibbs energy for viscous flow is defined for each ion, not each electrolyte. Note that Eq. (2.13) is consistent with the functional form of Eq. (2.12); we can write the right-hand side of Eq. (2.13) equivalently

as $\ln\left[(a_i^{ref})^{c_{0,i}} \cdot \exp\left(c_{1,i}\right)\right]$ and comparison to Eq. (2.12) identifies a_i^* as $a_i^* = (a_i^{ref})^{c_{0,i}+1} \cdot \exp\left(c_{1,i}\right)$. Each cation–anion pair is assigned a single coefficient, $c_{c,a}$ and $\Delta g_{c,a}^*$ is a function of the square root of molal ionic strength,

$$\frac{\Delta g_{c,a}^*}{RT} = c_{c,a}\sqrt{I}. \tag{2.14}$$

Molal ionic strength I is defined as

$$I = \frac{1}{2}\sum_{i}^{N} m_i z_i^2, \tag{2.15}$$

where m_i is the molality and z_i the integer (relative) electric charge of ion i. Equation (2.14) is inspired by similar expressions used for Pitzer-based ion activity coefficient expressions, such as those within AIOMFAC (Zuend et al., 2008).

Adding up the Gibbs energy contributions

The full expression for the molar Gibbs energy change for viscous flow of an aqueous solution is related to Eq. (2.4) and fits directly into the exponential function in Eq. (2.2); it consists of the weighted contributions from Eqs. (2.3), (2.13), and (2.14), covering all individual ions and all possible binary cation–anion combinations in the solution,

$$\frac{\Delta g^*}{RT} = x_{\mathrm{w}}\frac{\Delta g_{\mathrm{w}}^*}{RT} + \sum_{i=1}^{J}\left(x_i\frac{\Delta g_i^*}{RT}\right) + \sum_{c=1}^{J_c}\sum_{a=1}^{J_a}\left(\tau_{c,a}\,\frac{\Delta g_{c,a}^*}{RT}\right). \tag{2.16}$$

Here, $\tau_{c,a}$ is a special weighting term that accounts for contributions from all possible binary cation–anion pairs in a charge- and abundance-balanced manner. This can be accomplished by treating the aqueous solution as a mixture of charge-neutral cation–anion pairs with each cation combined with each anion, proportionally to the ion amounts involved. Consider the total positive charge in the aqueous electrolyte mixture, $\sum_{c=1}^{J_c} x_c \cdot z_c$, which is equivalent to the total negative charge, $\sum_{a=1}^{J_a} x_a \cdot |z_a|$, for an overall charge-neutral so-

lution. We can define the charge fraction ψ_a as the absolute amount of charge contributed by anion a relative to the sum of absolute charge contributions of all negative charges present (or alternatively, relative to the sum of all positive ones) in the mixture,

$$\psi_a = \frac{x_a \cdot |z_a|}{\sum_{a'=1}^{J_a} x_{a'} \cdot |z_{a'}|}, \tag{2.17}$$

and the weighting term,

$$\tau_{c,a} = \frac{x_c}{\nu_{c,el}} \cdot \psi_a. \tag{2.18}$$

$\tau_{c,a}$ represents the fractional amount of the hypothetical, neutral electrolyte component el consisting of cation c and anion a, where $\nu_{c,el}$ is the stoichiometric number of cations in a formula unit of this electrolyte. This treatment is further described in Section 2.7. Temporary cation–cation and anion–anion pairs are unlikely to form to the same extent because similarly charged ions will repel each other. Pitzer models show that to a first-order approximation, those interactions can be neglected (e.g. Zuend et al., 2008).

Some considerations bear mentioning. $\frac{\Delta g^*_w}{RT}$ is a unitless quantity related through Eq. (2.3) to the viscosity of pure water. At $298.15\,\mathrm{K}$, pure water has a viscosity of $8.9\times10^{-4}\,\mathrm{Pa\,s}$, and $\frac{\Delta g^*}{RT} = 3.44$. If the total Gibbs energy for viscous flow drops below this threshold, the Eyring equation will calculate a viscosity less than that of pure water. For certain aqueous electrolyte solutions that have a local viscosity minimum in the dilute range, this is a necessary condition. When a_i^{ref} values are less than one, the ionic contribution can become negative, allowing $\frac{\Delta g^*}{RT} < 3.44$. To avoid viscosity values that are too low, the cation–anion contribution may compensate by being more positive. This interplay of viscosity contributions from water, ions, and cation–anion interactions is delicate, and requires optimized coefficients. To avoid negative $\frac{\Delta g^*}{RT}$ and nonphysical behavior, we determined that all AIOMFAC-VISC coefficients should be positive real numbers.

2.3.4 Representing volume, charge, and hydration effects on viscosity

The effective size of the dissolved ions impacts the amount of Gibbs energy needed to activate viscous flow. Conceptually, if ions have small volumes, they slip relatively easily through the intermolecular network and into available/generated openings, displacing very few water molecules in the process; this would correspond to low viscosity. By contrast, large ions must displace more neighboring (solvent) molecules, which requires more energy temporarily and indicates higher viscosity. If an ion has a high charge density – the ratio of charge to ion volume – it will strongly attract water molecules into a temporary hydration shell, increasing the apparent size of the moving ion. Conversely, if an ion has low charge density, this hydration effect is reduced, sometimes negligible. In AIOMFAC-VISC, as part of the original AIOMFAC model, hydrated volumes are used for ions, ensuring that hydration effects are included where they are important. Ions in aqueous solutions with a strong hydration effect are termed "structure-making," while those with a large ionic volume and weak hydration effect are "structure-breaking" (Marcus, 2009). This behavior is also observed in the low-concentration mixture viscosity minimum observed in the viscosity curves of aqueous solutions of structure-breaking ions like K^+ and NH_4^+, but not those of structure makers like Li^+ and Mg^{2+} (as later shown in Fig. 2.2).

Molar volume of solution

We define the effective mean molar volume of the solution, V, as the mole-fraction-weighted mean of the pure-component molar volumes of the solvent and the dissolved ions, as in Eq. (2.5). A volume correction, c_v, is defined for the model and applied in all instances as

$$V = x_{\mathrm{w}} V_{\mathrm{w}} + c_v \sum_{i=1}^{J} x_i V_i. \tag{2.19}$$

The c_v term is included to account for potential discrepancies in attributed ionic volumes, some of which include partial hydration effects. AIOMFAC uses relative van der Waals volumes, which are calculated by solving for the volume of a sphere of radius r_c and dividing by $15.17 \times 10^{-6}\ \mathrm{m^3\,mol^{-1}}$, the volume of a reference subgroup (Abrams and Prausnitz, 1975; Fredenslund et al., 1975). The reference subgroup is used to calculate relative volumes for neutral molecules as well. For example, the relative volume for H_2O is 0.92 ($1.39564 \times 10^{-5}\ \mathrm{m^3\,mol^{-1}} / 15.17 \times 10^{-6}\ \mathrm{m^3\,mol^{-1}} = 0.92$). Values for the volumes and hydration numbers for the ions used in AIOMFAC-VISC are included in Table 2.1.

Table 2.1: Relative van der Waals ionic volume (R_t^H) parameters for cations and anions considering dynamic hydration. Table adapted from Zuend et al. (2008).

Species	$r_c(\mathrm{pm})^a$	N^{ADHb}	R_t	R_t^{Hc}
H^+	0	1.93	0.00	1.78
Li^+	76	0.58	0.07	0.61
Na^+	102	0.22	0.18	0.38
K^+	138	0.00	0.44	0.44
NH_4^+	161	0.00	0.69	0.69
Mg^{2+}	72	5.85	0.06	5.44
Ca^{2+}	123	2.10	0.31	2.24
Cl^-	181	0.00	0.99	0.99
Br^-	196	0.00	1.25	1.25
NO_3^-	179	0.00	0.95	0.95
HSO_4^-	215	0.00	1.65	1.65
SO_4^{2-}	215	1.83	1.65	3.34
I^-	220	0.00	1.77	1.77

[a] r_c values are the same as Zuend et al. (2008). For I^-, the r_c value is taken from Shannon (1976).
[b] Dynamic hydration effects are important for small and/or charge-dense ions. In other cases, the dynamic hydration number is zero. Dynamic hydration numbers are taken from Kiriukhin and Collins (2002).
[c] R_t^H values are taken from Table 1 of Zuend et al. (2008).

2.4 Data and Methods

2.4.1 Available viscosity measurements

At present, AIOMFAC can predict activity coefficients for seven cations (H^+, Li^+, Na^+, K^+, NH_4^+, Mg^{2+}, Ca^{2+}) and six anions (Cl^-, Br^-, NO_3^-, HSO_4^-, SO_4^{2-}, I^-), so we used only viscosity measurements for aqueous electrolyte systems that included combinations of these ions. Thirty-three such systems were used to fit the model. Ongoing work is extending AIOMFAC for additional ions of special relevance to aerosol particles, and future versions of AIOMFAC-VISC may include these ions. Data for 26 binary systems were aggregated by Laliberté (2007a); detailed references for all these data are included in that article and its electronic supplement. Data on seven ternary and quaternary systems were also used, provided by Laliberté (2007a) and Goldsack and Franchetto (1977a). These datasets include measurements at temperatures ranging from 263.15 to 427.15 K. Points at temperatures greater than 333.15 K were excluded from our model fit, to avoid biasing the model toward relatively high temperatures and because it is unlikely that aerosols will experience temperatures above 333.15 K in Earth's atmosphere. Ultimately, out of 6,669 available points in these 33 datasets, 6,130 were used to fit AIOMFAC-VISC.

Data availability varies considerably across systems. The systems with the most data are aqueous KCl, $NaCl$, $LiCl$, and $CaCl_2$ – each with more than 500 points. The mean number of data points per dataset is 200, but some systems like HCl, HNO_3, and $NaHSO_4$ each contain fewer than 20 points. As shown in Figs. 2.4 – 2.7, most viscosity measurements are clustered in the dilute concentration range. In fact, only 3 % of the viscosity measurements used to fit AIOMFAC-VISC are at mass fractions of water below 0.5. The highest available mass concentrations were for $Mg(NO_3)_2$, H_2SO_4, and NH_4NO_3, where measurements are available to mass fractions of water below 0.3 (solute mass fractions above 0.7). Some systems remain close to the viscosity of pure water throughout the concentration range, while others span multiple orders of magnitude – see the right two columns of

Table 2.2. For pure water at 298 K, $\log_{10}(\eta/\eta^{\circ}) = -3.054$. Structure-breaking electrolytes can be identified where $\log_{10}(\eta/\eta^{\circ})_{min}$ is less than -3.054. $Ca(NO_3)_2$ includes the greatest range, with viscosities between 10^{-4} and 10^{-1} Pa s, and approaching even higher values for the most concentrated solutions observed in laboratory experiments. While still in the liquid-like viscosity range, these high concentration data are of particular interest for aerosol modelling. More recently, techniques such as poke-and-flow, bead mobility, and holographic optical tweezers have enabled viscosity measurements for droplets (Reid et al., 2018). Due to their small size and absence of contact with solid surfaces, aqueous droplets often attain concentrations of solute exceeding the bulk solubility limits, suggesting higher viscosities are likely to occur in nature. Only a few datasets of this type exist, and we chose to use them for model verification rather than fitting.

Viscosity temperature dependence

Viscosity is strongly temperature dependent, and some viscosity models define their coefficients differently at each temperature, such as with the B-coefficients. AIOMFAC-VISC does not do this. We posit that the temperature-dependent pure-component viscosity of water already sufficiently captures the temperature dependence of aqueous electrolyte mixtures. Moreover, the AIOMFAC-VISC coefficients are assumed to be temperature-independent. In fitting AIOMFAC-VISC, we include measurements from 263.15 K to 333.15 K, and we use the same model coefficients at all temperatures. Including the data for multiple temperatures reduced the fit residuals considerably, when compared to a fit that only included data at temperatures at or near 298.15 K. Finally, AIOMFAC-VISC uses ion activity values from AIOMFAC that are optimized for a temperature of 298.15 K. Activity coefficients are weakly temperature dependent, so AIOMFAC-VISC predictions outside the 298 ± 30 K range may also be less reliable. To illustrate the temperature dependence of viscosity, measurements (and AIOMFAC-VISC predictions) are shown in Fig.

2.13 for several binary aqueous electrolyte solutions at selected temperatures within the range from 268 K to 328 K; see Section 2.7.

Error in viscosity measurements

Viscosity measurement error is rarely reported for bulk measurements, especially in publications before 1990. Where values do exist, they vary widely. For example, Roy et al. (2004) claims 0.05 % error in kinematic viscosity measurements. Abdulagatov et al. (2004) describes 1.5 % error in viscosity measurements for aqueous calcium nitrate solutions. Zhang and Han (1996) describe accuracy within 0.05 % for their viscosity measurements of aqeuous NaCl and KCl solutions. Wahab and Mahiuddin (2001) reported error of 0.5 % for aqueous calcium chloride solutions. A proxy for viscosity error is the scatter of our training data. Viscosity values measured at the same temperature and nearly identical concentrations show considerable scatter in multiple datasets (e.g., $\mathrm{K_2SO_4}$, $\mathrm{NaNO_3}$, and KBr – see Fig. 2.13), likely owing to different measurement techniques and/or measurement and transcription error. Laliberté (2007a) found the standard deviation of their viscosity residual to be 3.7 % of the average experimental viscosity for 74 datasets consisting of over 9,000 points in total. Due to the wide range of reported errors for viscosity and the scatter among similar measurement points, we decided to treat all measurements as if they included a 2 % error. This 2 % error is also included in the objective function used to fit the model. Displayed on a logarithmic scale, this error for bulk viscosity measurements is generally smaller than the plotted symbols, so error bars are mostly not shown. See Tables 2.2 and 2.3 for information on the temperature, concentration, and viscosity ranges of these datasets.

Table 2.2: Dataset information for binary aqueous electrolyte solutions used to fit the AIOMFAC-VISC electrolyte model. These data are a subset of the data aggregated by Laliberté (2007a, 2009).

Electrolyte	N	T_{min}	T_{max}	T_{mean}	$w_{\mathrm{w},min}$ [a]	$\log_{10}(\eta/\eta^\circ)^{\mathrm{b}}_{max}$	$\log_{10}(\eta/\eta^\circ)^{\mathrm{b}}_{min}$
KCl	585	278.15	333.15	304.82	0.6944	-3.012	-3.056
NaCl	479	278.15	333.15	304.58	0.7355	-2.751	-3.050
LiCl	569	268.15	333.15	300.24	0.5400	-1.827	-3.047
NH_4Cl	259	283.15	333.15	305.89	0.6757	-3.030	-3.058
$CaCl_2$	485	273.15	333.15	302.69	0.4868	-1.468	-3.047
$NaNO_3$	338	283.15	333.15	308.79	0.4479	-2.648	-3.049
NH_4NO_3	277	288.15	333.15	304.47	0.2151	-2.725	-3.072
$(NH_4)_2SO_4$	148	288.15	333.15	307.35	0.5371	-2.633	-3.047
Na_2SO_4	200	288.15	333.15	305.84	0.6687	-2.661	-3.050
NaBr	217	278.15	333.15	306.02	0.4595	-2.618	-3.050
$MgSO_4$	166	288.15	333.15	304.20	0.7015	-2.092	-3.050
$Mg(NO_3)_2$	214	273.15	323.15	300.52	0.5607	-2.153	-3.042
$MgCl_2$	319	288.15	333.15	307.59	0.6225	-1.892	-3.050
$LiNO_3$	88	273.15	333.05	299.87	0.3764	-1.878	-3.051
Li_2SO_4	147	278.15	333.15	303.30	0.7398	-2.305	-3.050
KNO_3	146	288.15	333.15	308.01	0.5050	-3.022	-3.061
KBr	319	273.15	333.15	302.19	0.5378	-3.024	-3.079
HCl	163	283.15	315.65	299.07	0.6400	-2.735	-3.050
HBr	11	273.15	298.15	288.60	0.8047	-3.017	-3.047
H_2SO_4	118	263.15	323.15	295.78	0.2180	-1.810	-3.048
$Ca(NO_3)_2$	132	263.15	333.00	307.08	0.3227	-1.538	-3.016
K_2SO_4	188	273.15	333.15	307.85	0.8453	-2.985	-3.050
KI	218	278.15	333.15	300.31	0.3726	-2.998	-3.093
NaI	150	278.15	332.41	300.14	0.3715	-2.513	-3.050
$NaHSO_4$	5	291.15	291.15	291.15	0.6249	-2.519	-2.954
HNO_3	16	277.15	298.15	290.40	0.6915	-3.037	-3.045

[a] $w_{\mathrm{w},min}$ is the minimum mass fraction of water, which corresponds to the highest solute concentration.
[b] These columns show the maximum and minimum values for $\log_{10}(\eta/\eta^\circ)$ at T = 298.15 K (or 291.15 K for $NaHSO_4$).
η° denotes unit viscosity (1 Pa s).

2.4.2 Simultaneously fitting the AIOMFAC-VISC electrolyte model

We used a combination of global optimization methods to simultaneously fit the c_v, $c_{0,i}$, $c_{1,i}$, and $c_{c,a}$ coefficients based on the ions and cation–anion pairs described by 33 aqueous electrolyte systems. All single-ion coefficients were fitted to data from multiple systems,

Table 2.3: Dataset information for ternary and quaternary aqueous electrolyte mixtures used to fit the AIOMFAC-VISC electrolyte model.

Electrolyte System	N	T	$w_{\mathrm{w},min}$	$\log_{10}(\eta/\eta^\circ)_{max}$	$\log_{10}(\eta/\eta^\circ)_{min}$
HCl + KCl + NaCl[a]	29	298.15	0.7627	-2.890	-3.046
$(NH_4)_2SO_4$ + Na_2SO_4[a]	6	298.15	0.6666	-2.697	-2.913
KBr + NaCl[a]	6	298.15	0.7031	-2.943	-3.044
KCl + NaCl[a]	6	298.15	0.7154	-2.921	-3.033
$(NH_4)_2SO_4$ + KCl[a]	6	298.15	0.8139	-2.964	-3.008
NaCl + KBr + $(NH_4)_2SO_4$[a]	6	298.15	0.6025	-2.859	-2.994
$CaCl_2$ + NaCl[b]	114	298.15	0.6957	-2.531	-3.048

η° denotes unit viscosity (1 Pa s)
[a] Goldsack and Franchetto (1977a)
[b] Laliberté (2007a)

e.g., c_{0,K^+} and c_{1,K^+} are simultaneously fitted to all data points that include the K^+ ion. First, we used a method described by Zuend et al. (2010) called "best-of-random differential evolution" (BoRDE), which is based on the Differential Evolution algorithm by Storn and Price (1997), a robust global optimization method. To implement BoRDE, we borrowed code from Zuend et al. (2010). After honing in on the coefficients with BoRDE, we switched to the constrained global optimization method (GLOBAL) by Csendes (1988), which implements the Boender–Rinnooy Kan–Stougie–Timmer algorithm in Fortran (Boender et al., 1982). The Fortran 90 version of GLOBAL is freely available online (Miller, 2003). GLOBAL identifies clusters of local minima to efficiently survey the parameter space, sometimes substantially improving upon the solution found by BoRDE. Inherent in both the GLOBAL and BoRDE fitting processes is an objective function, which is used to evaluate the model performance for a given set of the adjustable coefficients, where a smaller objective function value indicates a better model fit to the data. This function often takes the form of a residual or error equation, such as root mean square error, but it can also be customized to suit the data and the intended use of the model. Our objective function is described in Section 2.5.

2.4.3 Implementation for aqueous electrolyte systems

The AIOMFAC-VISC electrolyte model equations and coefficients have been implemented in Fortran and included as an optional module within the larger AIOMFAC model framework. The electrolyte model is incorporated alongside the aqueous organic viscosity model by Gervasi et al. (2020). AIOMFAC calculates activity coefficients for all components in a mixture based on activity coefficient contributions from long-range, middle-range, and short-range molecular interactions. Those three contributions include effects from dissolved ions, so it is essential that viscosity calculations for aqueous electrolyte solutions proceed after these contributions have been calculated. A number of input quantities are needed prior to calling the aqueous electrolyte solution viscosity module within AIOMFAC, including the calculation of the pure-component viscosity of water at given temperature, for which the parameterization by Dehaoui et al. (2015) is used. The mole fractions of water and the ions, the activity coefficients, and the relative ionic volumes are all available through the AIOMFAC interface, computed by various procedures within the AIOMFAC computer program. Equations (2.13) – (2.19) are then evaluated for the system and the mixture's dynamic viscosity is calculated via Eq. (2.2).

2.4.4 Generalizing AIOMFAC-VISC: three mixing models for organic–inorganic systems

In the aerosol context, particle phases will frequently contain a mixture of water, organic compounds, and inorganic ions. Therefore, we introduce a second extension to AIOMFAC-VISC, enabling viscosity predictions for mixtures consisting of water and an arbitrary number of organic compounds and inorganic ions. We note that, to date, viscosity measurement data for organic–inorganic mixtures are scarce, limiting comparisons between model predictions and measurements and the quantitative evaluation of different mixing approaches. Given our two distinct models – the one introduced above for pre-

dicting viscosity in organic-free aqueous electrolyte solutions and the one for electrolyte-free aqueous organic mixtures (Gervasi et al., 2020) – a coupled AIOMFAC-VISC mixing model for aqueous organic–inorganic mixtures can be designed in at least three ways.

In the following sections, we introduce three approaches for combining our aqueous electrolyte and aqueous organic viscosity models and discuss their differences in terms of physicochemical justification, implementation considerations and associated computational costs. Common to our approaches is the concept of describing the organic–inorganic system in each particle phase as a combination of two distinct subsystems: (1) an aqueous organic solution free of inorganic electrolytes, and (2) an organic-free aqueous electrolyte solution. Each subsystem may contain any number of components aside from water. The split into subsystems allows us to apply the appropriate organic- or electrolyte-specific viscosity model for each subsystem. For a given overall mixture composition, there is no obvious way, but several reasonable ways, by which the water content can be split into contributions to each subsystem; hence, different options emerge. Also, since water is the only common component present in the two subsystems, its modified properties (outlined in the following) can be considered to indirectly account for and mediate effects from interactions among ions and organics occurring in the actual (fully mixed) system.

Electrolyte-aware water mixed with organics

The first approach for computing the mixture viscosity, abbreviated as "aquelec", assumes that inorganic electrolytes dissolve exclusively in water as the predominant solvent for ions, which is typically a good approximation, especially under dilute aqueous solution conditions and/or in the absence of polar organic solvents. The key idea is to replace the pure component viscosity of water, which is used in the prediction of the mixture viscosity of the aqueous organic subsystem, by the viscosity predicted for the aqueous electrolyte subsystem. This electrolyte-aware "pseudo-pure" water property substitute

is then applied together with the properties of the organic components in the organic model, which is based in part on combinatorial-activity-weighted contributions of water and organics to determine mixture viscosity (Gervasi et al., 2020). In the aquelec mixing approach, the following steps are taken:

1. Adjust the ion molalities, which are by default defined by the molar ion amounts relative to $1\ \mathrm{kg}$ of water plus organics, $m_i = n_i/(W_\mathrm{w} + \sum W_{org})$, to be instead redefined relative to $1\ \mathrm{kg}$ of pure water as solvent, where $m_{i,aquelec} = n_i/W_\mathrm{w}$. In these expressions, n_i is the molar amount of ion i, and W_{org} and W_w are the masses of organic and water components, respectively, present in the total mixture. This can be expressed using a conversion factor, λ, as follows:

$$m_{i,aquelec} = \lambda\, m_i, \tag{2.20}$$

$$\lambda = W_\mathrm{w}/(W_\mathrm{w} + \sum W_{org}) = w_\mathrm{w}/(w_\mathrm{w} + \sum w_{org}). \tag{2.21}$$

2. Using $m_{i,aquelec}$, calculate ion activities with Eq. (2.9) and ionic strength with Eq. (2.15).

3. Redefine the ionic mole fractions relative to the organic-free aqueous electrolyte subsystem (subsystem 2). The full system ionic mole fractions, $x_i = n_i/(n_w + \sum n_{org} + \sum n_i)$, are replaced by the new "organic-free" ionic mole fractions, $x_{i,aquelec} = x_i/(x_\mathrm{w} + \sum x_{i'})$. Here, we introduce prime notation, e.g. i', to contrast the specific ion i with the index over which all ion molar amounts or mole fractions are summed.

4. Run the electrolyte model to calculate the viscosity of the aqueous electrolyte subsystem, ignoring organics.

5. Replace the pure-component viscosity of water in subsystem 1 with that of the aqueous electrolyte subsystem (electrolyte-aware water).

6. Set the mole fractions of ions to zero to avoid double-counting their effects and renormalize the mole fractions of water and organics for subsystem 1, so they become $x_{w,aquelec} = x_{\mathrm{w}}/(x_{\mathrm{w}} + \sum x_{org'})$ and $x_{org,aquelec} = x_{org}/(x_{\mathrm{w}} + \sum x_{org'})$.

7. Run the organic model (Gervasi et al., 2020) for the established mixture of electrolyte-aware water and the organic components to compute the viscosity of the organic–inorganic mixture as a whole.

Organics-aware water mixed with ions

As opposed to aquelec, another option, "aquorg", assumes that all water mixes with organic components to create an "organics-aware" water component that will replace pure water as the solvent of ions in the organic–inorganic mixture. Unlike aquelec, which first computes the interactions between ions and pure water, aquorg prioritizes the calculation for aqueous organic mixture viscosity. This mixing model is similar to aquelec, but the steps proceed in a different order, as follows:

1. Run the organic model (Gervasi et al., 2020) to calculate the viscosity for the aqueous organic subsystem, ignoring ions.

2. Replace the pure-component viscosity property of water in subsystem 2 with that of the aqueous organic subsystem (organics-aware water).

3. Add the mole fraction values of all organics to the mole fraction of water, and set the mole fractions of all organics to zero. Thus, the sum of moles of organics + moles of water is represented as moles of organics-aware water.

4. Run the electrolyte model for the mixture of organics-aware water and the inorganic ions to calculate viscosity of the organic–inorganic mixture.

Note that for the aquorg mixing mode, it is not necessary to modify the ion molalities because they are computed relative to $1\ \mathrm{kg}$ of organics-aware water, which for this pur-

pose is equivalent to the molality definition based on mass of water + organics in the denominator (as in the original mixture).

Splitting water content between organic and inorganic subsystems with a Zdanovskii–Stokes–Robinson mixing rule

The third mixing model is a Zdanovskii–Stokes–Robinson (ZSR) type mixing rule that preserves the organic-to-inorganic dry mass ratio (OIR). The ZSR mixing rule has been successfully used in many applications for the estimation of physical properties of a ternary mixture based on additive contributions from binary subsystems evaluated at the same water activity (i.e. RH under bulk equilibrium conditions) (Zdanovskii, 1936, 1948; Stokes and Robinson, 1966).

Unlike the other two mixing models described above, which only require a single call of the AIOMFAC program (for the computation of activity coefficients), the ZSR-style approach requires an iterative numerical solution: multiple runs are needed to pinpoint the mass fraction of water of the aqueous electrolyte and aqueous organic subsystems such that they yield the same water activity as that determined for the full mixture. As water activity is an output of an AIOMFAC calculation, this requires solving a non-linear equation in one unknown (mass fraction of water) for each subsystem.

Our ZSR-style mixing rule first calculates the RH of the full organic–inorganic system. Next, we split the full system into a salt-free aqueous organic subsystem (subsystem 1) and an organic-free aqueous electrolyte subsystem (subsystem 2). A modified version of Powell's hybrid method from the Fortran MINPACK library is used to calculate the water content and viscosity for the two subsystems at the target RH (Moré et al., 1980, 1984). Finally, the organic–inorganic mixture viscosity is estimated using a weighted arithmetic mean of the logarithms of subsystem viscosities, which is equivalent to a weighted geometric mean of the non-log subsystem viscosities. The expression for the mixing rule,

previously described in Song et al. (2021), is

$$\ln(\eta/\eta^\circ) = f_1 \ln(\eta_1/\eta^\circ) + f_2 \ln(\eta_2/\eta^\circ), \tag{2.22}$$

where f_1 and f_2 are the relative mass contributions from subsystem 1 and 2, respectively. η° denotes unit viscosity ($1\ \mathrm{Pa\,s}$). Expressions for f_1 and f_2 must ensure that the given OIR is preserved. Consider the mass W of the full system,

$$W = W_{org} + W_{el} + W_{\mathrm{w}}, \tag{2.23}$$

where org, el, and w denote organic, electrolyte (salt), and water components, respectively. Subsystem 1 contains all of the organic mass and subsystem 2 contains all of the salt mass; the water content can be split in a way that preserves OIR. By defining the mass of the subsystems as

$$W_1 = W_{org,1} + W_{\mathrm{w},1}, \tag{2.24}$$

$$W_2 = W_{el,2} + W_{\mathrm{w},2}, \tag{2.25}$$

$$W_{el} = W_{el,2}, \tag{2.26}$$

$$W_{org} = W_{org,1}, \tag{2.27}$$

OIR can be defined as

$$\mathrm{OIR} = \frac{W_{org}}{W_{el}} = \frac{W_{org,1}}{W_{el,2}} = \frac{w_{org,1} W_1}{w_{el,2} W_2}, \tag{2.28}$$

where $w_{org,1}$, $w_{el,2}$ are the mass fractions of the organic in subsystem 1 and salt in subsystem 2, respectively. The relative mass contributions are defined as

$$f_1 = \frac{W_1}{W_1 + W_2}, \tag{2.29}$$

$$f_2 = 1 - f_1. \tag{2.30}$$

Combining (2.29) and (2.28), we find that

$$f_1 = \frac{\mathrm{OIR} \times w_{el,2}}{w_{org,1} + \mathrm{OIR} \times w_{el,2}}. \tag{2.31}$$

Note that f_1 and f_2 are not constant for constant OIR and must be recomputed at every RH step. In dynamic simulations, it is expected that ZSR mixing will be computationally expensive due to the multiple calls to AIOMFAC and the iterative approach.

Advantages and disadvantages of the different mixing models

The perfect mixing model for viscosity will be physically justifiable, efficient, and accurate. The ZSR mixing rule to determine water content is built on established thermodynamic arguments, but its implementation is computationally more expensive than the other two mixing models. The "aquelec" and "aquorg" mixing models are about equally fast because neither requires an iterative approach, but the aquelec approach seems the more reasonable choice in terms of physicochemical justification. The primary assumption of the aquelec mixing model is that ions are likely to dissolve preferentially in water. By contrast, the aquorg mixing model implicitly treats organic components similar to water in terms of acting as solvent mass for the calculations in subsystem 2, which is not always a good assumption. In terms of accuracy, recently, the ZSR mixing rule has been shown to produce reasonable predictions of viscosity within an order of magnitude of measurements (Song et al., 2021). Predictions of organic–inorganic mixture viscosity with the three different approaches are compared in Section 2.5.7.

Activity coefficient calculations

Concurrently with the viscosity calculations, a full calculation is also carried out to determine the activity coefficients of all components/ions in the mixed organic–inorganic solution, as is also done in the absence of viscosity calculations with AIOMFAC. This

is necessary because the activity coefficients of the components/ions computed for the subsystems will differ from those computed for the full system.

2.5 Results and Discussion

Following a simultaneous fit of the AIOMFAC-VISC coefficients and implementation of the model in the AIOMFAC program, we found that AIOMFAC-VISC attained excellent agreement with bulk measurements and smooth extrapolations to low water contents for all 33 aqueous electrolyte systems. In this section, the values of the model parameters are reported and model design considerations are discussed first. Next, results are shown and discussed for binary, ternary, and quaternary aqueous electrolyte solutions, demonstrating the predictive capacity of the AIOMFAC-VISC aqueous electrolyte model. Finally, AIOMFAC-VISC predictions are shown for several aqueous inorganic and organic–inorganic mixtures for which recent aerosol techniques have been used to measure viscosity at target RH. The vast range of viscosities observed in nature, spanning more than 15 orders of magnitude, as well as the observed change of viscosity with composition, e.g. aerosol water content, or temperature, makes the use of a logarithmic viscosity scale useful; hence the frequent use of $\log_{10}(\eta/\eta^{\circ})$ in this work.

2.5.1 Fitting AIOMFAC-VISC for aqueous electrolyte sohttps://www.overleaf.com/

As discussed in Section 2.4.2, our method involved defining an objective function to fit the model. Our objective function is defined for each dataset and takes the form

$$f_{obj} = \sqrt{\frac{1}{N}\sum_{\iota=1}^{N}\left[\ln\left(\frac{\eta_{\mathrm{calc},\iota}+\sigma\cdot\eta_{\mathrm{exp},\iota}}{\eta_{\mathrm{exp},\iota}+\sigma\cdot\eta_{\mathrm{exp},\iota}}\right)\right]^2}, \tag{2.32}$$

where ι in the data point index, N is the number of data points, and σ is an uncertainty threshold. Summing the f_{obj} values over all datasets and dividing by the sum gives the relative error contribution for each dataset. $Ca(NO_3)_2$, LiCl, and $CaCl_2$ contribute the largest shares of error, as shown in Fig. 2.1. Our objective function includes a 2 % uncertainty term ($\sigma = 0.02$) to characterize an approximate viscosity measurement error. However, it does not include additional consideration for the asymmetric distribution of measurements across different ranges in concentrations or temperature at which the measurements were collected, which may affect the distribution of the objective function value.

Through trial and error, we arrived at a framework that includes two coefficients per ion, one per cation–anion pair, and one volume correction term that is used for all model calculations. With the 33 datasets used in our fit, 55 unique coefficients were identified, describing 13 ions and 28 cation–anion interactions. Several $c_{c,a}$ coefficients were not covered by the measured systems but can still occur in AIOMFAC-VISC predictions; therefore, coefficients from similar cation–anion pairs were substituted in these cases, serving as approximations, e.g., $c_{Li^+,Br^-} = c_{Li^+,Cl^-}$. All values of these coefficients are included in Tables 2.4 and 2.5, and replacements are noted in Table 2.8. The fitted c_v value is 1.071559.

2.5.2 Model design considerations

How many parameters are needed to accurately and meaningfully model the viscosity of a binary aqueous electrolyte solution? The answer to this question is not so simple, as some parameters are defined for the entire model, whereas others are solute- or ion-specific. The model by Lencka et al. (1998) extends the Jones–Dole framework by including ionic B-coefficients and introducing a third term for species–species interaction that is proportional to the square of molar ionic strength. It requires three parameters: two ionic B-coefficients and one binary interaction parameter. As in the Jones–Dole equation, however, the B-coefficients are temperature-dependent and some aqueous electrolyte so-

lutions require extra parameters for the species–species interaction term. By contrast, the Laliberté (2007a) model uses six coefficients per electrolyte. Temperature dependence is embedded in their expression for solute viscosity, and their use of six coefficients per electrolyte is able to correlate viscosity over a broad concentration range (with limited extrapolation beyond the concentration and temperature range of available measurement data), meaning that the full flexibility of his model is contained in a single equation.

We argue that AIOMFAC-VISC is more predictive and versatile than Laliberté's model because AIOMFAC-VISC's single-ion coefficients are simultaneously fitted with data from multiple aqueous electrolyte systems and can be used to estimate viscosity in binary and multi-electrolyte systems for which no laboratory viscosity measurements exist. Furthermore, Laliberté's mixing model, a mass-fraction-weighted mixing rule, requires knowledge of the solute concentration in terms of associated electrolyte units. Atmospheric aerosols often include multiple dissociated cations and anions. In the Laliberté model, predicting the viscosity of multi-ion solutions introduces ambiguity because the ions would need to be mapped into electrolyte units. For example, an aqueous mixture of KBr and NaCl and an aqueous mixture of KCl and NaBr have different calculated viscosities according to the Laliberté model, even though the ionic concentrations are identical. AIOMFAC-VISC can sidestep this problem of electrolyte ambiguity with its unique design. A further aspect of the use of single-ion contributions to viscosity, via Eq. (2.13), is the dependence on predicted single-ion activities in this expression, allowing the resulting Δg_i^* term to indirectly account for non-ideal mixing effects. This means that effects of specific counter-ions on a particular ion in the solution, at otherwise the same solute molality, are considered. Therefore, while the single-ion coefficients ($c_{0,i}$ and $c_{1,i}$) are the same for ion i in any mixture, the interaction effects of the reference solvent and of other ions present are at least partially accounted for.

Table 2.4: AIOMFAC-VISC ion coefficients, $c_{0,i}$ and $c_{1,i}$ [a].

Ion	c_0	c_1
H^+	3.581548×10^{-2}	4.776127
Li^+	1.732975×10^{-2}	4.945788
K^+	6.667175×10^{-1}	8.183509×10^{-1}
Na^+	8.527540×10^{-1}	5.809605
Ca^{2+}	5.890048×10^{-1}	1.484627×10^{1}
NH_4^+	9.284003×10^{-2}	1.180242×10^{-1}
Mg^{2+}	1.010392×10^{-11}	2.031022×10^{1}
Cl^-	2.568961×10^{-2}	6.071930
Br^-	2.902611×10^{-1}	4.319046
NO_3^-	4.667751×10^{-1}	4.980264
SO_4^{2-}	8.914285×10^{-1}	2.663463×10^{1}
HSO_4^-	2.411699×10^{-3}	5.891363
I^-	1.753617×10^{-1}	7.536467×10^{-1}

[a] The number of digits listed reflects approximately the precision used in the model code; it does not imply that all digits are significant figures.

2.5.3 Comparison of AIOMFAC-VISC and the Laliberté model for aqueous electrolyte systems

Due to the substantial overlap in fitted datasets, we use the Laliberté model as a benchmark for AIOMFAC-VISC, both with respect to its closeness of fit to bulk viscosity measurements and its extrapolative behavior. We fitted AIOMFAC-VISC to available bulk viscosity measurements, resulting in excellent agreement for all datasets, although that is less apparent when compared with the Laliberté model. For example, in Fig. 2.1, we see that in panels (b) – (d) and for all systems, AIOMFAC-VISC's error magnitude is greater than that of the Laliberté model. This is expected, because the Laliberté model is fitted to aqueous electrolyte solutions (with six specific, independent parameters for each system) as opposed to AIOMFAC-VISC, which includes ion-specific coefficients shared among many electrolyte systems. The left-most panel displays mean bias error (MBE) for the

Table 2.5: AIOMFAC-VISC cation–anion pair coefficient, $c_{c,a}$ [a].

Cation	Anion	Value	*	Cation	Anion	Value	*
H^+	Cl^-	2.003688×10^{-1}		H^+	SO_4^{2-}	9.550524×10^{-2}	
Li^+	Cl^-	1.872142		Li^+	SO_4^{2-}	3.597352	
K^+	Cl^-	1.010392×10^{-11}		K^+	SO_4^{2-}	1.010392×10^{-11}	
Na^+	Cl^-	1.010392×10^{-11}		Na^+	SO_4^{2-}	4.218441×10^{-1}	
Ca^{2+}	Cl^-	1.814174		Ca^{2+}	SO_4^{2-}	2.975663	*
NH_4^+	Cl^-	4.042758×10^{-1}		NH_4^+	SO_4^{2-}	1.010392×10^{-11}	
Mg^{2+}	Cl^-	2.892983		Mg^{2+}	SO_4^{2-}	2.975663	
H^+	Br^-	9.100048×10^{-2}		H^+	HSO_4^-	8.984473×10^{-1}	
Li^+	Br^-	1.872142	*	Li^+	HSO_4^-	1.772322	*
K^+	Br^-	2.945562×10^{-1}		K^+	HSO_4^-	1.772322	*
Na^+	Br^-	1.370821×10^{-1}		Na^+	HSO_4^-	1.772322	
Ca^{2+}	Br^-	1.814174	*	Ca^{2+}	HSO_4^-	1.772322	*
NH_4^+	Br^-	1.010392×10^{-11}		NH_4^+	HSO_4^-	1.772322	*
Mg^{2+}	Br^-	2.892983	*	Mg^{2+}	HSO_4^-	1.772322	*
H^+	NO_3^-	1.010392×10^{-11}		H^+	I^-	9.100048×10^{-2}	*
Li^+	NO_3^-	1.145880		Li^+	I^-	1.872142	*
K^+	NO_3^-	1.089775		K^+	I^-	1.779648	
Na^+	NO_3^-	3.335819×10^{-1}		Na^+	I^-	1.527357	
Ca^{2+}	NO_3^-	2.741503		Ca^{2+}	I^-	1.814174	*
NH_4^+	NO_3^-	8.258685×10^{-1}		NH_4^+	I^-	4.042758×10^{-1}	*
Mg^{2+}	NO_3^-	2.096909		Mg^{2+}	I^-	2.892983	*

[a] The number of digits listed reflects approximately the precision used in the model code; it does not imply that all digits are significant figures.
* denotes cation–anion pairs for which no measurements were available. In these cases, the fit parameter of a similar pair is substituted, e.g., Ca^{2+} Br^- uses the same value as Ca^{2+} Cl^-. See Table 2.8 for full list of substitutions made.

binary systems defined in Table 2.2. MBE is defined as

$$\mathrm{MBE} = \frac{1}{N}\sum_{\iota=1}^{N}\left(\log_{10}\left[\eta_{\mathrm{calc},\iota}/\eta^\circ\right] - \log_{10}\left[\eta_{\mathrm{exp},\iota}/\eta^\circ\right]\right), \tag{2.33}$$

where N is the number of points in each dataset, $\eta_{\mathrm{calc},\iota}$ is the calculated viscosity value of either AIOMFAC-VISC or the Laliberté model, and $\eta_{\mathrm{exp},\iota}$ is the viscosity value reported in the measurements at point ι. Overall, AIOMFAC-VISC does not exhibit systematic bias, with negative bias for 15 datasets and positive bias for 11 datasets. The magnitudes of MBE are generally larger for AIOMFAC-VISC than for the Laliberté model, which again

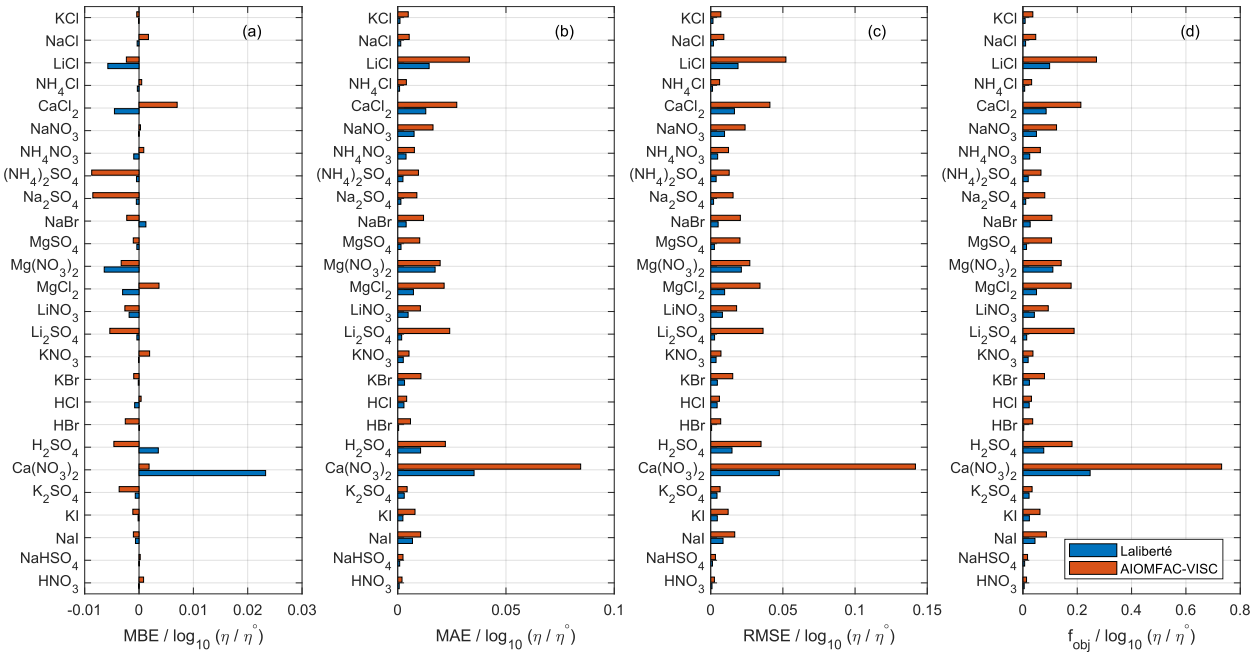

Figure 2.1: Comparison of AIOMFAC-VISC and the Laliberté model in terms of (a) mean bias error, (b) mean absolute error, (c) root mean square error, and (d) custom objective function value used to fit AIOMFAC-VISC. See Table 2.2 for information on number of data points, the ranges of temperature, concentration, and viscosity for each dataset. η° denotes unit viscosity ($1\ \mathrm{Pa\,s}$).

is expected. Two systems stand out, however: $\mathrm{CaCl_2}$ and $\mathrm{Ca(NO_3)_2}$, both of which show positive bias. These two datasets include some of the highest viscosity values among the available measurements, which is a factor in their large contributions to the overall objective function error. It is also worth noting that the Laliberté model has its largest value of MBE for $\mathrm{Ca(NO_3)_2}$, suggesting that this system is difficult to model, even when using more adjustable parameters. Figs. 2.1b,c show mean absolute error (MAE), which is defined as

$$\mathrm{MAE} = \frac{1}{N}\sum_{i=1}^{N} |\log_{10}\left[\eta_{\mathrm{calc},\iota}/\eta^\circ\right] - \log_{10}\left[\eta_{\mathrm{exp},\iota}/\eta^\circ\right]|, \tag{2.34}$$

and root mean square error (RMSE), which is defined as

$$\mathrm{RMSE} = \sqrt{\frac{1}{N}\sum_{i=1}^{N} \left(\log_{10}\left[\eta_{\mathrm{calc},\iota}/\eta^\circ\right] - \log_{10}\left[\eta_{\mathrm{exp},\iota}/\eta^\circ\right]\right)^2}. \tag{2.35}$$

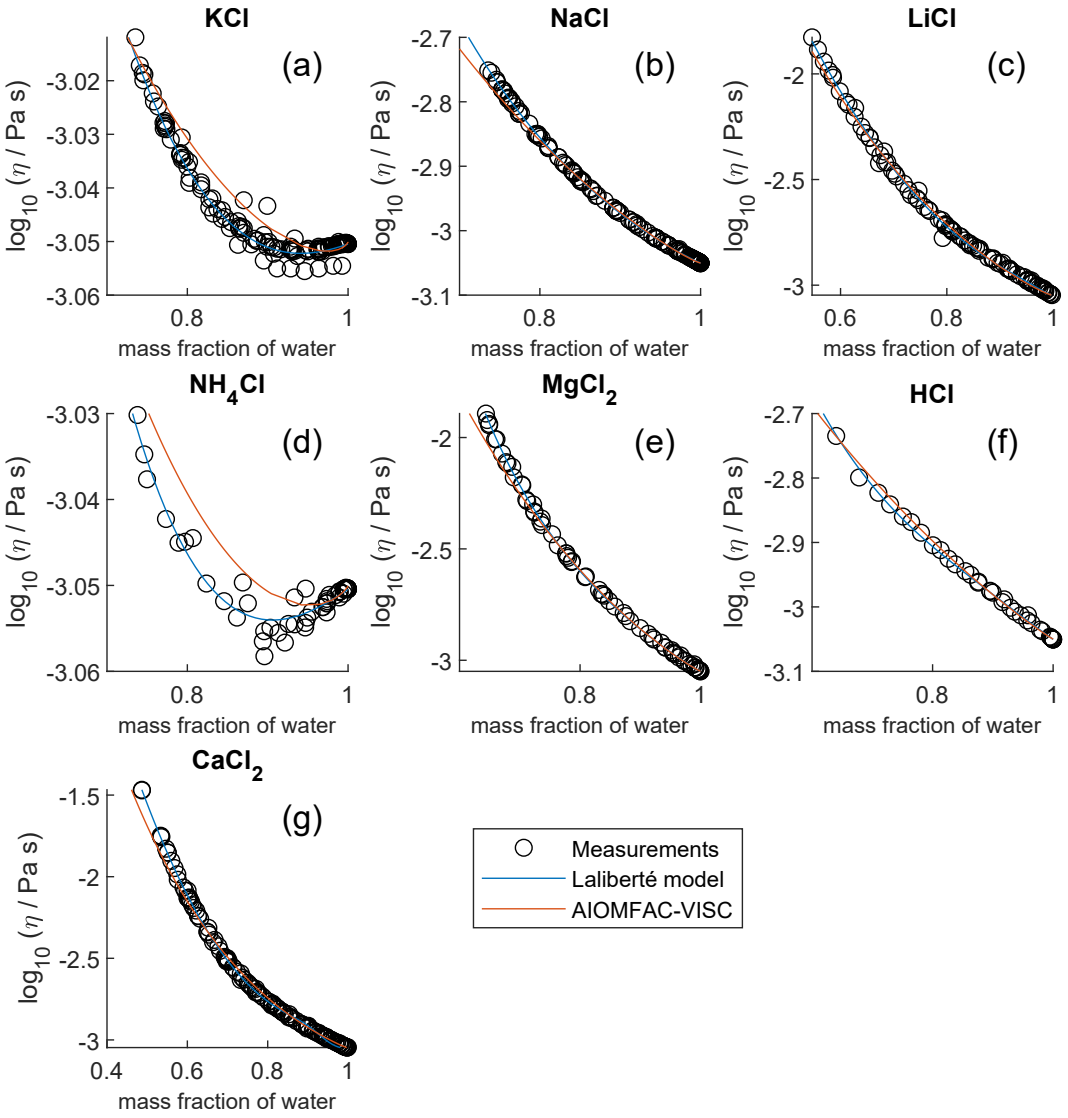

Figure 2.2: Comparison of closeness of fit for aqueous chloride salts/acids. Zooms are adjusted in each panel to best fit the measurements. See Fig. 2.4 for model extrapolations throughout the full concentration range and Table 2.2 for information on the measurement data.

The most significant deviations from the measurements are for $\mathrm{Ca(NO_3)_2}$, LiCl, and $\mathrm{CaCl_2}$. The values of the root mean square error and the custom objective function, Eq. (2.32), are presented in panels (c) and (d) of Fig. 2.1, and reinforce the same result.

In Fig. 2.2, the panels are zoomed in individually to show how AIOMFAC-VISC and the Laliberté model align with the bulk viscosity measurements over the covered concen-

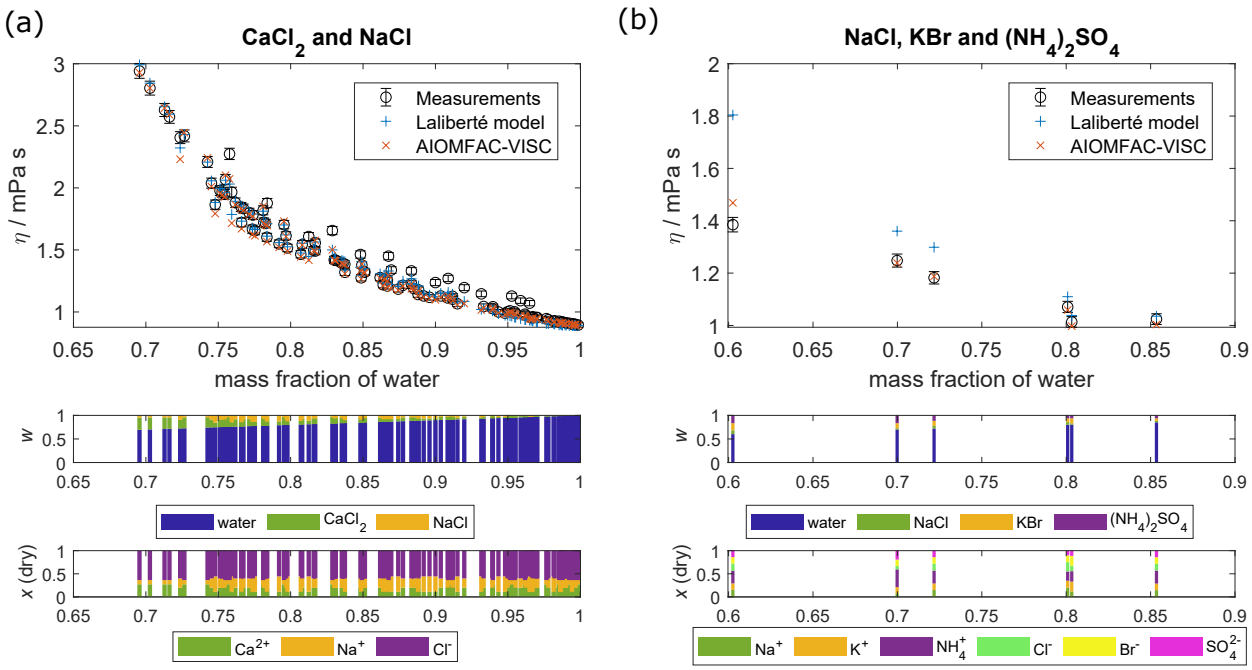

Figure 2.3: Comparison of AIOMFAC-VISC predictions and Laliberté model results with measured data points for aqueous mixtures of more than one electrolyte: (a) $\mathrm{CaCl_2}$ and NaCl and (b) NaCl, KBr, and $(\mathrm{NH_4})_2\mathrm{SO_4}$. Middle panel bar graphs show the mass fractions (w) with respect to non-dissociated electrolytes and lower bar graphs show the ion mole fractions with water excluded, $x(\mathrm{dry})$. 2% vertical error bars are included to represent viscosity measurement error.

tration and viscosity ranges. KCl (Fig. 2.2a) and $\mathrm{NH_4Cl}$ (Fig. 2.2d) show local minima in their viscosity curves, a characteristic of structure-breaking electrolytes. In these panels, as well as for $\mathrm{CaCl_2}$ (Fig. 2.2g), it is evident that the Laliberté model has a closer fit with the measurements. KCl and $\mathrm{NH_4Cl}$ have extremely narrow vertical axes, effectively only showing viscosities close to that of pure water. Some panels, by contrast, span more than one order of magnitude, with AIOMFAC-VISC slightly underpredicting the highest viscosity measurements.

2.5.4 Closeness of fit to bulk viscosity measurements for ternary and quaternary aqueous electrolyte mixtures

Viscosity measurements for mixtures of water and more than one electrolyte are less common than those of binary aqueous solutions, but they better demonstrate AIOMFAC-VISC's predictive capacity. The datasets in Table 2.3 were used to fit AIOMFAC-VISC, but were not fitted by the Laliberté model. Therefore, we effectively compare AIOMFAC-VISC's fit for these multi-ion solutions to the Laliberté mixing model, the latter being a simple mass-fraction-weighted mixing rule. As these measurements are on the same order of magnitude as the viscosity of pure water, we change the units on the vertical axis to $\mathrm{mPa\,s}$, and include 2% error bars.

Figure 2.3 shows AIOMFAC-VISC predictions alongside measurements and Laliberté-calculated values for two aqueous multi-ion solutions. As with the binary solution results, AIOMFAC-VISC and the Laliberté model agree closely at high mass fraction of water and diverge as the solute concentration increases. In Fig. 2.3a, there is close agreement between the two models and the measurements. This behavior is expected due to the strong model–measurement agreement of binary NaCl and binary $\mathrm{CaCl_2}$. Considering the much larger viscosity scale that is typical for atmospheric aerosol cases, this level of agreement with the measurements is very encouraging. For the ternary aqueous electrolyte mixture $\mathrm{H_2O}$ + $\mathrm{CaCl_2}$ + NaCl in Fig 2.3a, the Laliberté model requires 12 parameters, or six for each electrolyte. AIOMFAC-VISC, by contrast, includes two coefficients for each individual ion, reducing the number needed in the case of common ions, in this case $\mathrm{Cl^-}$. For this example, AIOMFAC-VISC depends on only 9 of the fitted coefficients, namely 2 for $\mathrm{Ca^{2+}}$, 2 for $\mathrm{Na^+}$, 2 for $\mathrm{Cl^-}$, 1 for the first cation–anion pair, $\mathrm{Ca^{2+}}$–$\mathrm{Cl^-}$, 1 for the second cation–anion pair, $\mathrm{Na^+}$–$\mathrm{Cl^-}$, plus 1 for the volume correction term. In Fig 2.3b, the number of data points is much smaller, but AIOMFAC-VISC outperforms the Laliberté model for 5 out of 6 points. This is likely due to AIOMFAC-VISC's more comprehensive treatment for dissolved ions and cation–anion pairs and because we used these data during

the simultaneous fit of the aqueous electrolyte model. While the Laliberté model characterizes three electrolytes and their mixing, AIOMFAC-VISC accounts for nine potential cation–anion pairs and weights their contributions in a stoichiometrically consistent way. Additional ternary and quaternary aqueous electrolyte mixtures are shown in Figs. 2.11 and 2.12, located in Section 2.7. In each of those multi-ion cases involving either chloride, bromide and chlorides, sulfate, or sufate and chloride as anions, AIOMFAC-VISC performs as well or better than the Laliberté model. Given that those datasets were used in the overall fit of the AIOMFAC-VISC parameters, this is not unexpected. Nevertheless, those successful representations of multi-ion cases, though limited by experimental data, provide confidence in AIOMFAC-VISC's ability to predict the viscosities of multi-ion solutions of various compositions.

2.5.5 Extrapolative behavior for binary aqueous electrolyte solutions at room temperature

In Figures 2.4 through 2.7, we compare AIOMFAC-VISC predictions with extrapolations from the Laliberté model at 298 K. Agreement between AIOMFAC-VISC and the Laliberté model is excellent within the range of available measurements for each system, which are plotted as black circles. Outside of this range, the models diverge, sometimes to a large degree. It is worth noting that crystallization is inhibited/neglected in both the AIOMFAC-VISC and the Laliberté model calculations, resulting in (mostly) smooth curves throughout the concentration range. Also, the Laliberté model occasionally depicts spurious behavior outside of the measurement range. When the Laliberté model exceeds its applicability limit, which is provided for each electrolyte in Laliberté (2007a), it can sometimes produce negative viscosity values as output; on a logarithmic viscosity scale plot, these deviations are indicated by a sharp discontinuity in the viscosity curve. AIOMFAC-VISC never predicts negative viscosity values, but at exceedingly low water activity, AIOMFAC by default stops its calculations when run for a single curve covering

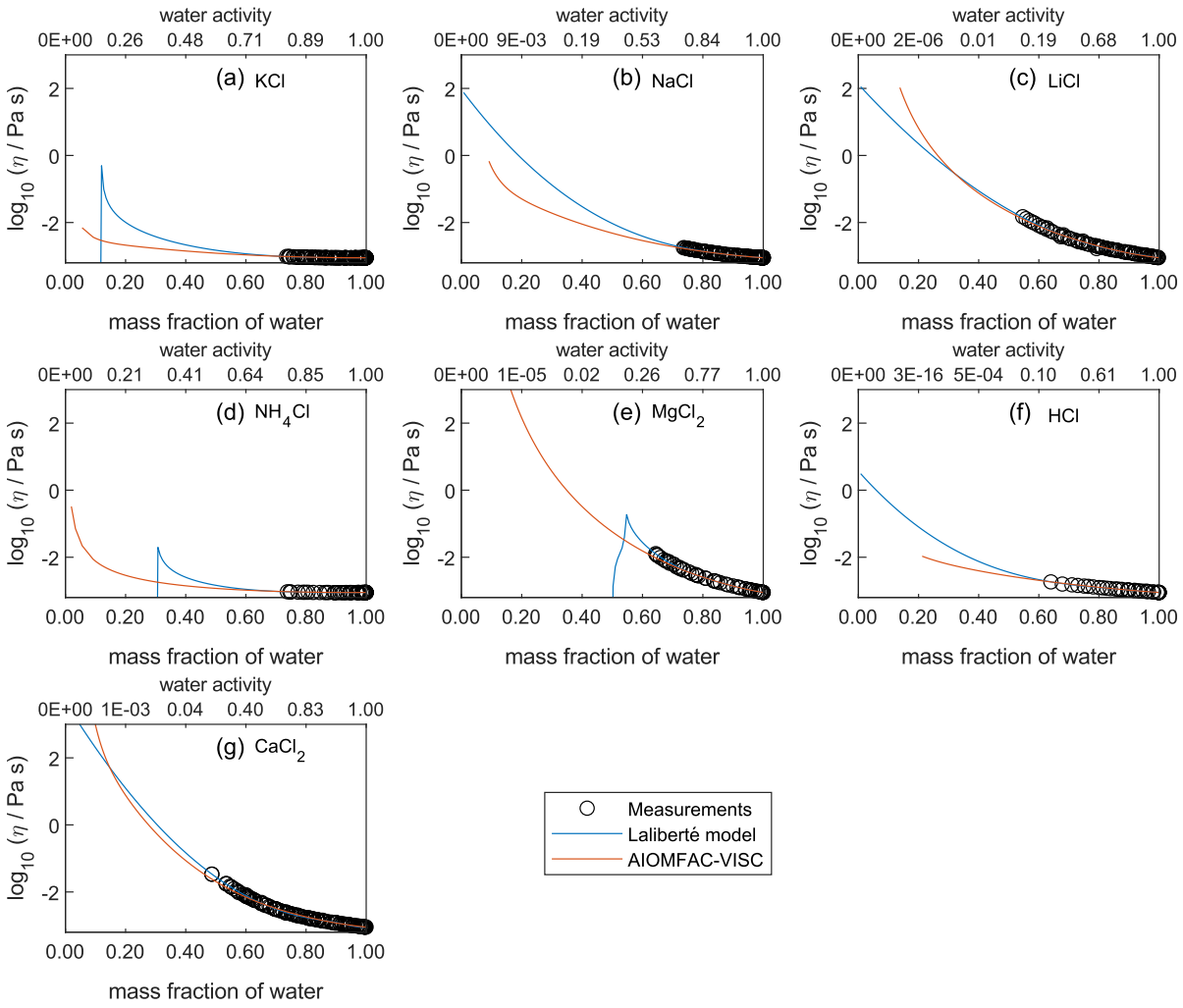

Figure 2.4: Comparison of the Laliberté model, AIOMFAC-VISC, and viscosity measurements versus mass fraction of water (bottom axis) and AIOMFAC-predicted water activity (top axis) for binary solutions of chloride salts at 298 K: (a) KCl; (b) NaCl; (c) LiCl; (d) NH_4Cl; (e) $MgCl_2$; (f) HCl; (g) $CaCl_2$. Sharp discontinuities on the Laliberté model curve indicate extrapolation to non-physical values; extrapolated values should not be used beyond such points, which are outside of the valid concentration ranges provided by Laliberté (2007a). AIOMFAC-VISC predictions are not shown for concentrations corresponding to exceedingly low predicted water activity ($a_w < 10^{-12}$), so the curve sometimes stops abruptly. Neither model accounts for potential crystallization of the solute (enabling predictions for extremely high ionic strengths). The values in the top axis are rounded to two significant digits.

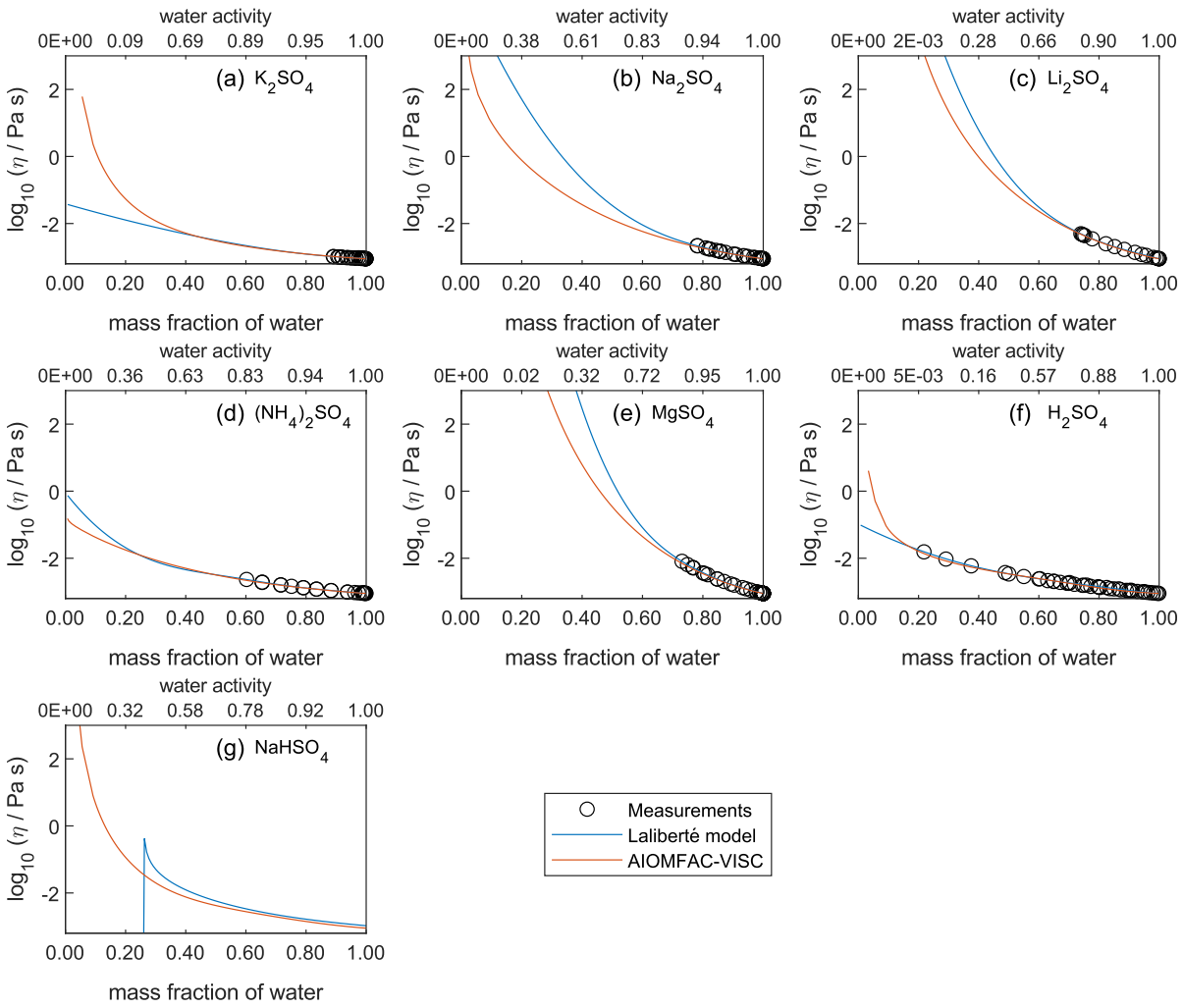

Figure 2.5: Comparison of the Laliberté model, AIOMFAC-VISC, and viscosity measurements versus mass fraction of water (bottom axis) and AIOMFAC-predicted water activity (top axis) for binary solutions of sulfate salts at 298 K: (a) K_2SO_4; (b) Na_2SO_4; (c) Li_2SO_4; (d) $(NH_4)_2SO_4$; (e) $MgSO_4$; (f) H_2SO_4; (g) $NaHSO_4$. No measurements were available for $NaHSO_4$ at 298.15 K. See also caption to Fig. 2.4.

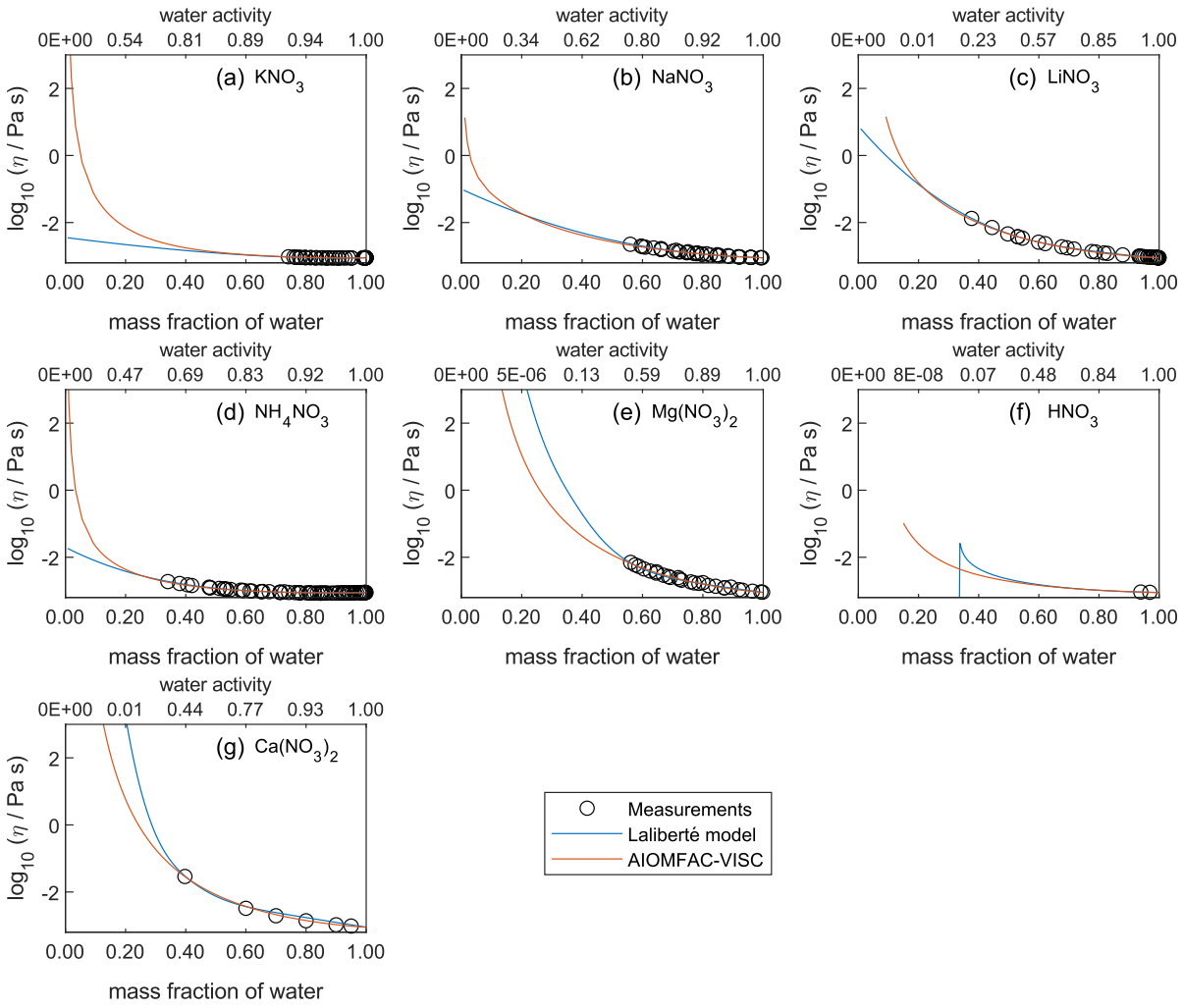

Figure 2.6: Comparison of the Laliberté model, AIOMFAC-VISC, and viscosity measurements versus mass fraction of water (bottom axis) and AIOMFAC-predicted water activity (top axis) for binary solutions of nitrate salts at 298 K: (a) KNO_3; (b) $NaNO_3$; (c) $LiNO_3$; (d) NH_4NO_3; (e) $Mg(NO_3)_2$; (f) HNO_3; (g) $Ca(NO_3)_2$. See also caption to Fig. 2.4.

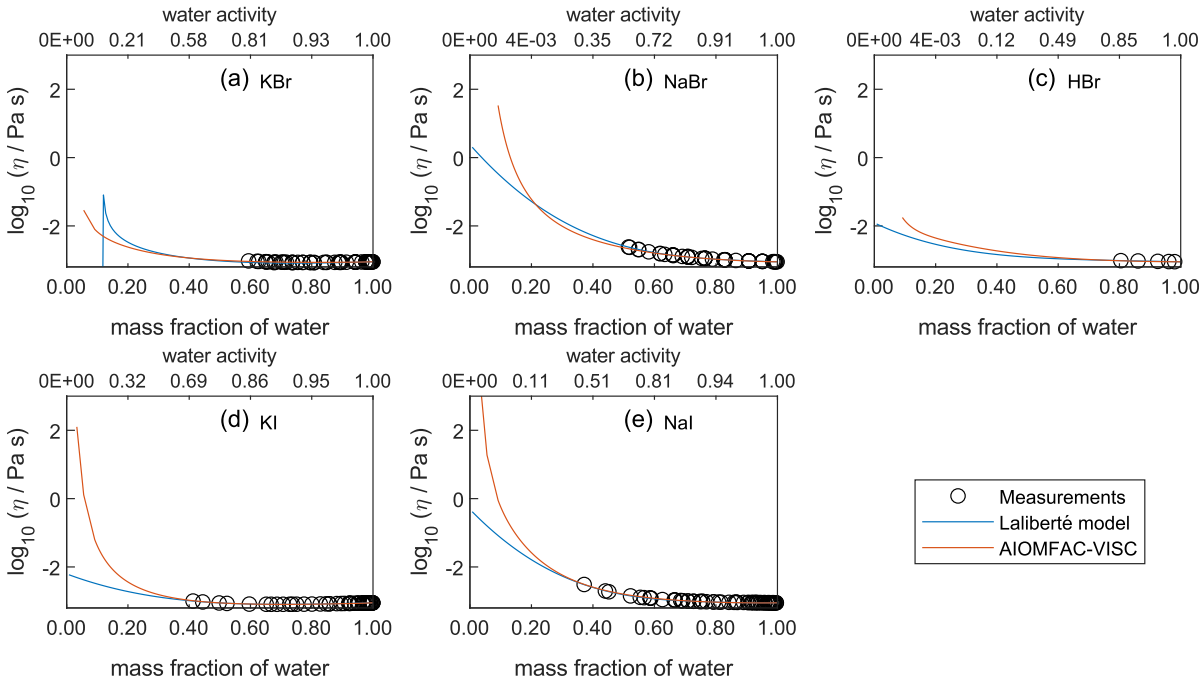

Figure 2.7: Comparison of the Laliberté model, AIOMFAC-VISC, and viscosity measurements versus mass fraction of water (bottom axis) and AIOMFAC-predicted water activity (top axis) for binary solutions of bromide and iodide salts at 298 K: (a) KBr; (b) NaBr; (c) HBr; (d) KI; (e) NaI. See also caption to Fig. 2.4.

output from dilute to concentrated conditions. This is justified since the resulting water activities at low w_{w} would be for conditions far beyond a realistic equilibrium RH in the atmosphere (or other environments). Water activity and w_{w} vary differently for different aqueous electrolyte solutions as shown by comparing the upper and lower horizontal axis of each panel; so, the exact point at which the model output was stopped is different for each aqueous electrolyte solution, but is typically below $w_{\mathrm{w}} = 0.2$.

For aqueous chloride salts/acids, (Fig. 2.4), AIOMFAC-VISC and the Laliberté model agree closely, generally to within one order of magnitude (even outside the concentration range of the measurements). For NaCl and LiCl (Fig. 2.4b,c), the Laliberté model projects a near linear increase in $\log_{10}$ viscosity below the w_{w} threshold of the measurements, while the AIOMFAC-VISC predictions include a more steep increase in viscosity below $w_{\mathrm{w}} = 0.4$, likely due to higher relative influence of the ionic-strength-dependent

cation–anion viscosity contributions. For KCl, NH_4Cl, and $MgCl_2$ (Fig. 2.4a,d,e), the Laliberté model shows spurious behavior outside of the measurement range. In these cases, the AIOMFAC-VISC predictions are preferable because the curves remain smooth.

In Figs. 2.5 – 2.7, AIOMFAC-VISC and the Laliberté model continue to agree closely. The AIOMFAC-VISC curve for H_2SO_4 (Fig. 2.5f) includes a notch below $w_w = 0.2$, which indicates a relatively sharp change in the bisulfate dissociation degree as predicted by AIOMFAC for the sulfate–bisulfate equilibrium in that system. For $Ca(NO_3)_2$ (Fig. 2.6g), the AIOMFAC-VISC curve closely fits the measurement points, but predicts a lower viscosity than the Laliberté model below $w_w = 0.4$.

Due to the lack of viscosity measurements at low mass fraction of water and the tendency for salts to crystallize at high concentration, it is difficult to determine quantitatively which model/curve, if any, is correct for any given case. What is clear, however, is that AIOMFAC-VISC provides an excellent level of accuracy in the composition range where measurement data are available and can be used in place of the Laliberté model in most instances.

2.5.6 Comparing AIOMFAC-VISC with aqueous inorganic aerosol surrogate mixtures

Unlike bulk viscosity measurement techniques, which determine viscosity for known composition (e.g. mass fractions), recent aerosol and/or microscopic droplet viscosity measurement techniques characterize viscosity with respect to known equilibrium water activity (RH) instead. A limited number of measurements of this type are available; we present results for three aqueous nitrate salts, $Ca(NO_3)_2$, $Mg(NO_3)_2$, and $NaNO_3$.

Figure 2.8 shows the predicted viscosity of aqueous nitrate salts over the full RH range with AIOMFAC-VISC model sensitivity represented by the upper and lower dashed curves. AIOMFAC-VISC model sensitivity is defined by a 2% change in the aerosol water mass

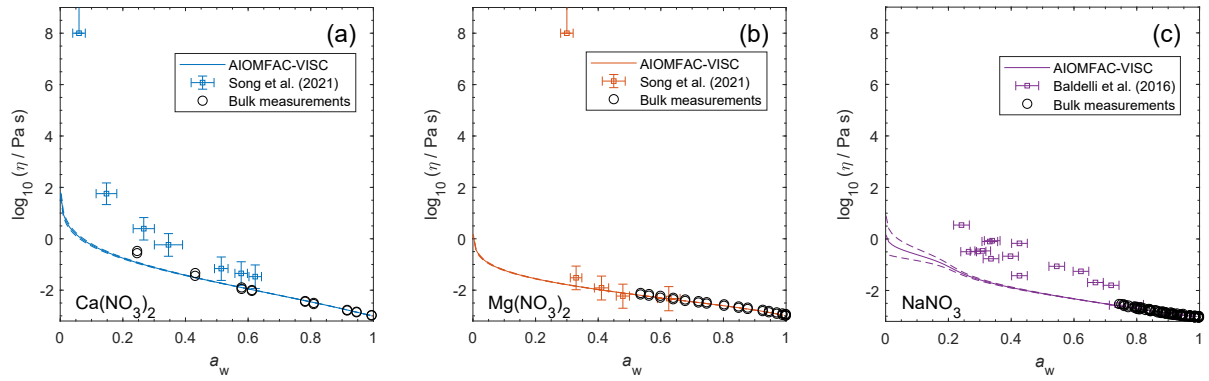

Figure 2.8: Viscosity predictions for aerosol surrogate mixtures containing nitrate salts at varying water activity, a_w (RH). Model sensitivity, defined by a 2% change in aerosol water content, is shown in dashed curves. Bulk measurements (used to fit AIOMFAC-VISC) were collected at defined concentrations and converted to a_w using AIOMFAC; the points collected at temperatures between 293±5 K are shown. Song et al. (2021) used poke-and-flow and bead mobility techniques. Baldelli et al. (2016) used holographic optical tweezers. Unlike the bulk measurements, these were not used to fit AIOMFAC-VISC.

fraction, described in the supporting information of Gervasi et al. (2020). In the case of aqueous $Ca(NO_3)_2$ (Fig. 2.8a), disagreement between the two measurement datasets is noticed, especially at lower water activities. AIOMFAC-VISC shows positive bias relative to the bulk measurements, and it shows better agreement with the aerosol measurements between $a_w = 0.65$ and $a_w = 0.3$. It is possible that these bulk measurements understate viscosity for aqueous $Ca(NO_3)_2$, which would mean that the large model deviation for this system is not necessarily so bad. This is especially intriguing because the aerosol measurements were not used to fit AIOMFAC-VISC. In the case of $Mg(NO_3)_2$ (Fig. 2.8b) the aerosol measurements largely agree with the bulk measurements, and AIOMFAC-VISC correctly characterizes nearly every point. In both Fig. 2.8a,b there is one outlying data point at low a_w with a stated viscosity value at 10^8 Pa s. In fact, Song et al. (2021) used 10^8 Pa s as the upper limit for their viscosity measurements. Such a high value reported may be best explained by the crystallization of $Ca(NO_3)_2$ or $Mg(NO_3)_2$, but using the poke-and-flow measurement technique, it is difficult to distinguish between glasses, gels, and crystallized aerosols. Crystallization is inhibited in the shown AIOMFAC-VISC pre-

dictions, likely explaining the divergence from those high-viscosity measurement points. Our AIOMFAC-based equilibrium model is capable of providing liquid–liquid and solid–liquid equilibrium calculations, but viscosity prediction would not be possible for the solid phase. In the case of $\mathrm{NaNO_3}$ (Fig. 2.8c), there is rather poor agreement between the bulk measurements and the aerosol measurements by Baldelli et al. (2016). At $a_\mathrm{w} < 0.2$, the uncertainty of the AIOMFAC-VISC prediction for $\mathrm{NaNO_3}$ widens considerably, indicating that small changes in solution water content can greatly affect both the water activity and viscosity predictions. Indeed, a 2 % change in mass fraction of water corresponds to a much larger change in water activity for $\mathrm{NaNO_3}$ (Fig. 2.6b) than for $\mathrm{Ca(NO_3)_2}$ (Fig. 2.6e) or $\mathrm{Mg(NO_3)_2}$ (Fig. 2.6g). The upper sensitivity limit of this prediction indicates that $\mathrm{NaNO_3}$ particles of semi-solid viscosity might be observed below $\sim$ 10 % RH, which corresponds to an observation of non-crystalline viscous $\mathrm{NaNO_3}$ in particle rebound experiments by Li et al. (2017).

Although viscosity measurements are not available, aqueous $\mathrm{MgSO_4}$ particles have been observed as highly viscous liquids and/or (non-Newtonian) gels (Li et al., 2017; Cai et al., 2015; Richards et al., 2020a). AIOMFAC-VISC predicts uniquely high viscosity values for aqueous $\mathrm{MgSO_4}$, and a transition to a semi-solid viscosity below $a_\mathrm{w} = 0.4$. Richards et al. (2020a) differentiate gels from Newtonian liquids by the presence of an abrupt change in microrheology and the lack of shape relaxation (on practical experimental timescales). It is not possible to verify these findings with the present version of AIOMFAC-VISC, which does not explicitly include consideration of liquid-to-gel phase transitions, and they clearly merit further study.

Nevertheless, the theory behind AIOMFAC-VISC can account to some extent for the unique behavior of aqueous $\mathrm{MgSO_4}$. $\mathrm{Mg^{2+}}$ and $\mathrm{SO_4^{2-}}$ are both doubly charged ions, which likely attract water molecules into long-lasting hydration shells. As RH decreases, free water molecules evaporate from the particle, leaving behind the hydrated ions. These hydrated cations and anions agglomerate, forming chains and reducing the flow of molecules.

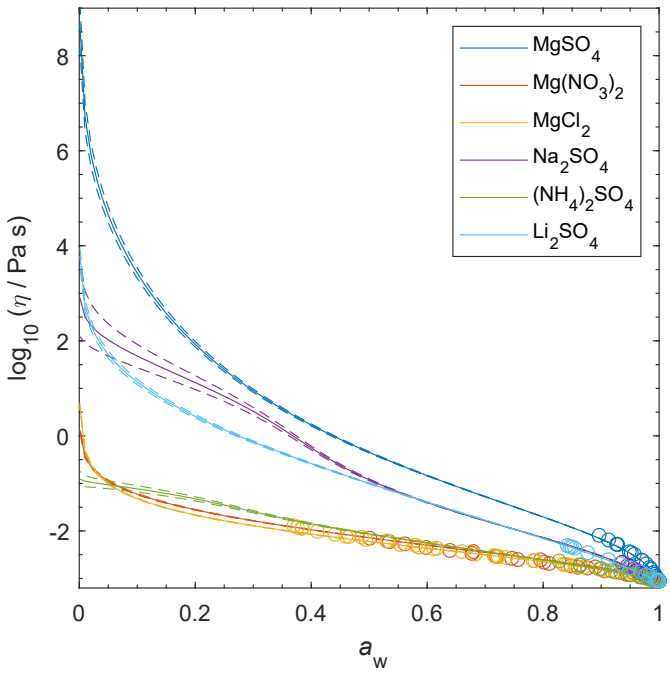

Figure 2.9: AIOMFAC-VISC predicted viscosity for selected binary aqueous electrolyte solutions at 298.15 K. Model sensitivity (dashed curves) shows the impact of a 2 % variability in determined aerosol water content at stated a_{w}. Bulk measurements are shown as circles, with colors matching their respective electrolytes.

No other aqueous electrolytes that we used to fit AIOMFAC-VISC included two doubly charged ions, but we did include other electrolytes which contained $\mathrm{Mg^{2+}}$ or $\mathrm{SO_4^{2-}}$, and we have plotted them alongside $\mathrm{MgSO_4}$ in Fig. 2.9. Below $a_{\mathrm{w}} = 0.4$, the $\mathrm{MgSO_4}$ predicted viscosity is consistently higher than that of the other binary aqueous solutions shown by at least two orders of magnitude in viscosity. Predicted viscosities for the other binary aqueous solutions remain below the semi-solid threshold (10^2 Pa s) throughout the RH range. $\mathrm{MgCl_2}$ and $\mathrm{Mg(NO_3)_2}$ produce nearly identical predictions, suggesting that the effects of chloride and nitrate anions are similar, or that ion interactions in $\mathrm{MgSO_4}$ are more important than those of other magnesium-containing electrolytes. On the other hand, the predictions for the other sulfate-containing electrolytes differ substantially from each other. $\mathrm{Na_2SO_4}$ and $\mathrm{Li_2SO_4}$ produce higher predicted viscosities than $\mathrm{(NH_4)_2SO_4}$, suggesting that the inclusion of a more charge-dense cation as the counter-ion to $\mathrm{SO_4^{2-}}$ results in slightly higher viscosity.

2.5.7 Comparing AIOMFAC-VISC with aqueous organic–inorganic aerosol surrogate mixtures

Measurements are available for aqueous mixtures of sucrose with $Ca(NO_3)_2$, $Mg(NO_3)_2$, and $NaNO_3$. Sucrose is commonly used as a proxy for secondary organic aerosol because it has a similar oxygen-to-carbon ratio as highly oxidized organic aerosol components and viscosity and related diffusivity data are available in the literature (Evoy et al., 2019). In Fig. 2.10, AIOMFAC-VISC viscosity predictions are tested for these systems at varying water activity, providing a comparison of the three organic–inorganic mixing approaches described in Section 2.4.4. Each of these mixing approaches predicts viscosities between those of the relevant sucrose-free aqueous nitrate salt solution and the aqueous (salt-free) sucrose solution (plotted in grey). As the OIR increases, the mixture viscosity prediction approaches that of aqueous sucrose and as the OIR decreases, the prediction tends toward the viscosity of the aqueous nitrate salt. Figure 2.10a,b show cases for an OIR of 1, while Figure 2.10c,d are for an OIR of 1.5 and 4, respectively. The reported error in viscosity for the Song et al. (2021) measurements can be as large as an order of magnitude, much larger than the typical reported error for bulk measurements. AIOMFAC-VISC's model sensitivity is mostly contained within the width of the error bars. Viscosity error bars for Fig. 2.10c,d were not available.

The aquelec mixing model predictions appear to agree best with the measurements for 1:1 sucrose–$Ca(NO_3)_2$ (Fig. 2.10a) and 60:40 sucrose–$NaNO_3$ (Fig. 2.10c), while the ZSR-style mixing rule performs best for 1:1 sucrose–$Mg(NO_3)_2$ (Fig. 2.10b) and 80:20 sucrose–$NaNO_3$ (Fig. 2.10d). In Fig. 2.10b, aquelec predicts values within the uncertainty of the measurements between 70 and 30 % RH, but underpredicts the measurements between 20 and 10 % RH. The aquorg mixing model consistently predicts lower viscosity values than the other two mixing models, and this negative bias is exacerbated at low RH. The measurements for binary solutions of some salts include abrupt increases in viscosity at low RH (5 % for $Ca(NO_3)_2$ and 35 % for $Mg(NO_3)_2$, as shown in Fig. 2.8). This could be the

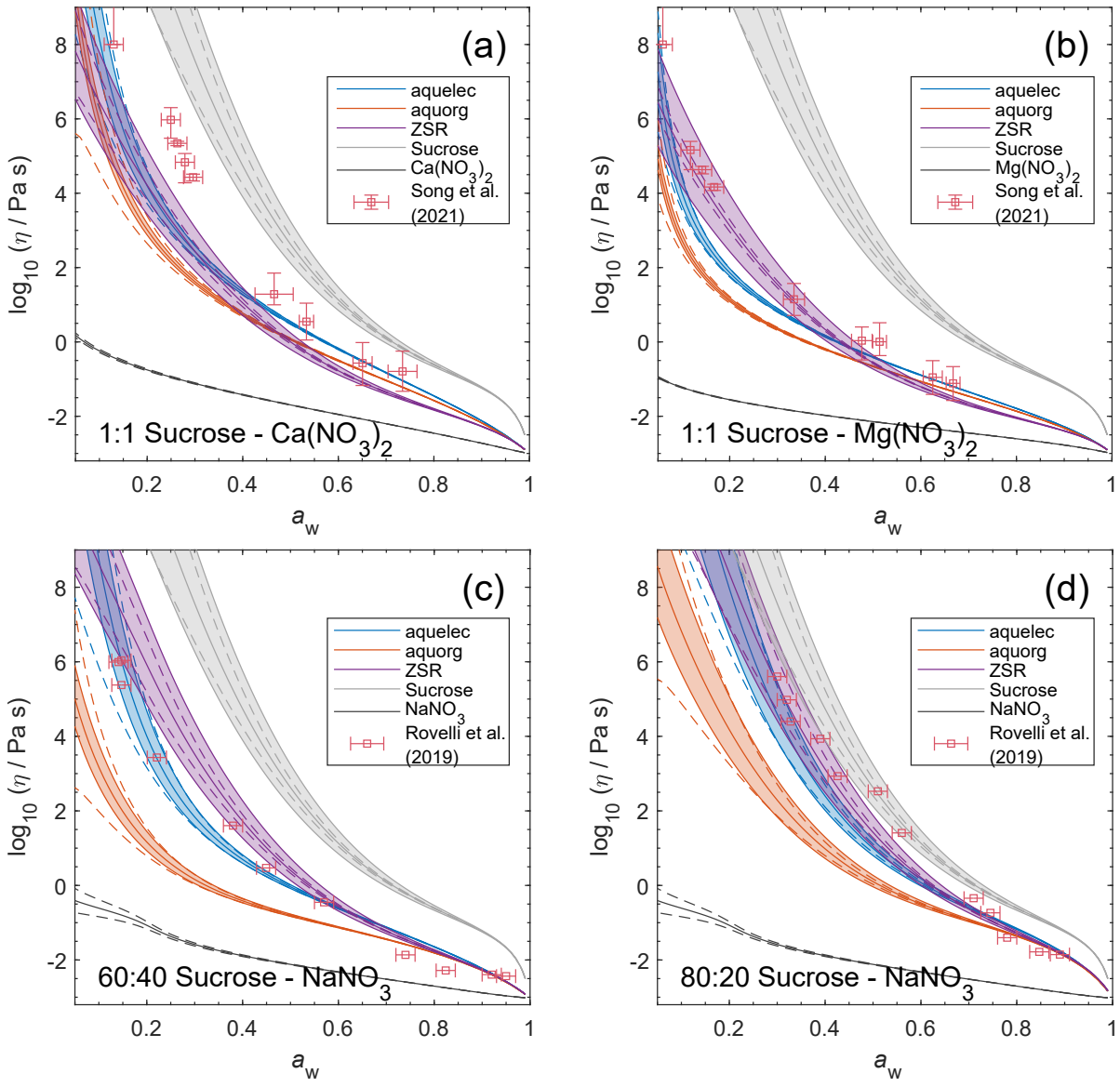

Figure 2.10: Viscosity predictions for aerosol surrogate mixtures containing sucrose and nitrate salts at varying water activity, a_w (RH), with a prescribed organic-to-inorganic dry mass ratio (OIR). Three mixing models – aquelec, aquorg, and ZSR – are shown alongside the viscosity measurements. Model sensitivity, defined by the impact of a 2 % change in aerosol water content, is shown by the dashed curves. Shaded regions show the potential viscosity prediction error introduced by a $\pm 5\,\%$ error in the glass transition temperature of sucrose. AIOMFAC-VISC predictions are also included for the binary aqueous sucrose and aqueous nitrate salt systems, which correspond to the organic and inorganic subsystems used in each mixing model (see Section 2.4.4).

result of crystallization of the salt, a glass transition, or a gel transition during the experiments. Regardless, when mixed with sucrose, this abrupt viscosity increase appears to be inhibited. Richards et al. (2020b) found that ternary organic–inorganic mixtures containing certain doubly charged cations had higher viscosity than the corresponding salt-free aqueous organic mixture, but AIOMFAC-VISC would not be able to produce such results without further additions for organic–ion effects (a potential subject of future work). Of the three systems shown here, the viscosity of aqueous sucrose is consistently higher than the ternary mixture throughout the RH range.

In terms of computational speed, the ZSR mixing model takes approximately five to six times longer than aquelec or aquorg (see Tables 2.6 and 2.7 in Section 2.7). In dynamic simulations that may require repeated calls to AIOMFAC, such as kinetic multilayer diffusion models, this time difference may be an important consideration.

2.6 Conclusions

A new predictive model has been developed and parameterized to enable calculations of the viscosity of aqueous electrolyte solutions. Furthermore, the earlier framework for aqueous organic mixtures has been successfully coupled with the electrolyte model, providing a more general model applicable to aqueous organic–inorganic mixtures. The AIOMFAC-VISC electrolyte model is based on Eyring's absolute rate theory for viscous flow, which has been used previously to describe the viscosity of aqueous electrolyte solutions up to approximately 10 molal. A new expression for the molar Gibbs energy of activation for viscous flow for aqueous electrolyte solutions was introduced, defining contributions from individual ions and present cation–anion pairs. Thirty-three aqueous electrolyte systems comprising 6,130 data points were used to simultaneously fit the AIOMFAC-VISC electrolyte model. AIOMFAC-VISC's ionic coefficients are fitted using viscosity measurements at a wide range of concentrations as opposed to classical

B-coefficients, which were fitted at dilute conditions. AIOMFAC-VISC closely fits the available data and produces smooth predictive extrapolations, performing as well as Laliberté's model, considered a benchmark. AIOMFAC-VISC also aligns with more recent measurements of aerosol surrogate mixtures containing aqueous nitrate salts.

Three mixing approaches were examined; aquelec and ZSR were found to be approximately equally accurate. The aquelec mixing approach is suggested as the preferred choice for use of AIOMFAC-VISC within dynamic (kinetic) simulations of viscosity or diffusion, because it is less computationally expensive. AIOMFAC-VISC's full functionality allows predictions of aqueous organic–inorganic mixtures consisting of an arbitrary number of organic compounds and inorganic ions. Future experimental work on a wider range of compositions and a more diverse set of multicomponent systems (presently highly data-limited) may provide data and insights that could allow further refinements of the organic–inorganic mixing model. AIOMFAC-VISC may also provide an opportunity to further explore aerosol phase state, especially gel transitions, which have become a topic of interest in aerosol studies (Song et al., 2021; Richards et al., 2020a,b).

2.7 Supplementary Information

2.7.1 Derivation for cation–anion viscosity contribution weighting

This section further describes the cation–anion contribution treatment introduced in Section 2.3.3. For multi-ion mixtures, a special weighting must be derived to be fully consistent with all potential cation–anion pairings and such that there is no double counting of the contributions of a specific ion when paired up with the various anions. This can be accomplished by treating the aqueous solution as a mixture of (dissolved) charge-neutral cation–anion pairs, with each cation combined with each anion proportionally to the charge-weighted ion amounts involved in the solution overall. That is, we can think

of the ions present in the solution as being the result of dissolving various possible electrolyte components (initially). The goal here is to provide a means of quantifying a "fair" share of each possible electrolyte component (as a binary, charge-balanced cation–anion unit) in a clearly defined manner. Consider the total of positive charges in the aqueous electrolyte mixture, $\sum_{c=1}^{J_c} n_c \cdot z_c$, which is equivalent in magnitude to the total of negative charges, $\sum_{a=1}^{J_a} n_a \cdot |z_a|$, for an overall charge-neutral solution. We can define the charge fraction ψ_a as the absolute amount of charge contributed by anion a relative to the sum of absolute charge contributions of all negative charges present (or alternatively, relative to the sum of all positive ones) in the mixture,

$$\psi_a = \frac{n_a \cdot |z_a|}{\sum_{a'=1}^{J_a} n_{a'} \cdot |z_{a'}|}, \tag{2.36}$$

and introduce a cation–anion pair contribution weighting term,

$$\tau'_{c,a} = \frac{n_c}{\nu_{c,el}} \cdot \psi_a. \tag{2.37}$$

$\tau'_{c,a}$ represents the fractional amount of the hypothetical, neutral electrolyte component el consisting of cation c and anion a, where $\nu_{c,el}$ is the stoichiometric number of cations in a formula unit of this electrolyte. Note that there is only one such cation–anion combination per specific type of cation and anion. In Eqs. (2.17 – 2.37), x_c can be understood as the molar amount of cation c in solution, normalized by the total molar amount of all species. Therefore, it is clear that either using an absolute, mole-based scaling ($\tau'_{c,a}$) or a relative mole-fraction-based scaling ($\tau_{c,a}$, Eq. 2.18) offer a description of the amounts of each "input" electrolyte component contributing ions to a solution (or unit amount of solution). The prime notation is removed in Eqs. (2.17 – 2.18) to indicate that mole-fraction-based scaling is used.

To illustrate the utility and consistency of this approach, consider an example mixture containing 2 $\mathrm{mol\ NaCl}$, 9 $\mathrm{mol\ MgSO_4}$, and 3 $\mathrm{mol\ NaBr}$ in water. If all these electrolytes

completely dissociate (as is assumed by AIOMFAC), the resulting solution composition can be written as 5 $\mathrm{mol\ Na^+}$, 2 $\mathrm{mol\ Cl^-}$, 9 $\mathrm{mol\ Mg^{2+}}$, 9 $\mathrm{mol\ SO_4^{2-}}$, and 3 $\mathrm{mol\ Br^-}$ in solution. From these two cations and three anions, the following six charge-neutral cation–anion pairs can be formed: NaCl, $\mathrm{MgSO_4}$, NaBr, $\mathrm{MgCl_2}$, $\mathrm{Na_2SO_4}$, and $\mathrm{MgBr_2}$.

When describing the viscosity contributions from cation–anions pairs using Eq. (2.14), in order to avoid excessive weight being attributed to a certain ion pair, we advocate that one should strive for an unbiased representation of the solution by means of accounting for all possible contributions from cation–anion pairs in a charge-equivalent manner of weighting. As a counter-example, an excessive, unbalanced weighting would likely occur if one were to pair, e.g., all $\mathrm{Mg^{2+}}$ with all $\mathrm{SO_4^{2-}}$ present, thereby giving a relatively high weight to the $c_{\mathrm{Mg^{2+},SO_4^{2-}}}$ parameter (Eq. 2.14) in the mixture viscosity calculation. This may bias this model prediction toward the viscosity of aqueous $\mathrm{MgSO_4}$ (at the same ionic strength) and the resulting value may be substantially different from a viscosity calculation involving a different choice of cation–anion pairing, such as if we had first combined all $\mathrm{Na^+}$ with $\mathrm{SO_4^{2-}}$ and only the remainder of sulfate with magnesium. Hence, the specific sequence of pairing the cations with the anions into hypothetical electrolyte components will lead to different viscosity predictions by the model (if several options are possible), making the prediction dependent on seemingly arbitrary choices and thereby ambiguous. Such ambiguity can be circumvented by introducing our $\tau'_{c,a}$-based weighting, in which a fractional amount of each cation is combined with a fractional amount of each anion, proportional to the charge-weighted amounts of the anions and the stoichiometry of the electrolyte unit formed.

In our example, $\mathrm{Na^+}$ is paired with all anions ($\mathrm{Cl^-}$, $\mathrm{SO_4^{2+}}$, $\mathrm{Br^-}$) in such a way that the largest fractional amount of $\mathrm{Na^+}$ is paired with $\mathrm{SO_4^{2+}}$, the second-largest amount is paired with $\mathrm{Br^-}$, and the smallest amount is paired with $\mathrm{Cl^-}$. We can calculate the exact proportions for $\mathrm{Na^+}$ by computing the charge-based fractions for each counter-ion (anion)

using Eq. (2.36). Here,

$$\psi_{\mathrm{Cl^-}} = \frac{n_{\mathrm{Cl^-}} \cdot |z_{\mathrm{Cl^-}}|}{\sum_{J_c} n_c \cdot z_c} = \frac{2 \cdot |-1|}{(5 \cdot 1) + (9 \cdot 2)} = \frac{2}{23} \tag{2.38}$$

$$\psi_{\mathrm{Br^-}} = \frac{n_{\mathrm{Br^-}} \cdot |z_{\mathrm{Br^-}}|}{\sum_{J_c} n_c \cdot z_c} = \frac{3 \cdot |-1|}{(5 \cdot 1) + (9 \cdot 2)} = \frac{3}{23} \tag{2.39}$$

$$\psi_{\mathrm{SO_4^{2-}}} = \frac{n_{\mathrm{SO_4^{2-}}} \cdot |z_{\mathrm{SO_4^{2-}}}|}{\sum_{J_c} n_c \cdot z_c} = \frac{9 \cdot |-2|}{(5 \cdot 1) + (9 \cdot 2)} = \frac{18}{23}, \tag{2.40}$$

while for each of the $\mathrm{Na^+}$–anion pairs, Eq. (2.37) yields

$$\tau'_{\mathrm{Na^+,Cl^-}} = \frac{n_{\mathrm{Na^+}}}{\nu_{\mathrm{Na^+,NaCl}}} \cdot \psi_{\mathrm{Cl^-}} = \frac{5}{1} \cdot \frac{2}{23} = \frac{10}{23} \tag{2.41}$$

$$\tau'_{\mathrm{Na^+,Br^-}} = \frac{n_{\mathrm{Na^+}}}{\nu_{\mathrm{Na^+,NaBr}}} \cdot \psi_{\mathrm{Br^-}} = \frac{5}{1} \cdot \frac{3}{23} = \frac{15}{23} \tag{2.42}$$

$$\tau'_{\mathrm{Na^+,SO_4^{2-}}} = \frac{n_{\mathrm{Na^+}}}{\nu_{\mathrm{Na^+,Na_2SO_4}}} \cdot \psi_{\mathrm{SO_4^{2-}}} = \frac{5}{2} \cdot \frac{18}{23} = \frac{45}{23}. \tag{2.43}$$

$\tau'_{c,a}$ can be calculated for the other five potential charge-neutral cation–anion pairs, yielding $\tau'_{\mathrm{Mg^{2+},SO_4^{2-}}} = \frac{162}{23}$; $\tau'_{\mathrm{Na^+,Br^-}} = \frac{15}{23}$; $\tau'_{\mathrm{Na^+,SO_4^{2-}}} = \frac{45}{23}$; $\tau'_{\mathrm{Mg^{2+},Cl^-}} = \frac{18}{23}$; and $\tau'_{\mathrm{Mg^{2+},Br^-}} = \frac{27}{23}$. These values add up in a way that is stoichiometrically consistent, e.g., extracting the $\mathrm{Na^+}$ amount from these hypothetical electrolyte component amounts yields $\tau'_{\mathrm{Na^+,Br^-}} + \tau'_{\mathrm{Na^+,Cl^-}} + 2 \cdot \tau'_{\mathrm{Na^+,SO_4^{2-}}} = \frac{15+10+90}{23} = 5\,\mathrm{mol\,Na^+}$. In our implementation of this approach, the normalized, mole-fraction-based version of $\tau_{c,a}$ is used directly in Eq. (2.16).

2.7.2 Computational efficiency of organic–inorganic mixing approaches

We tested the speed of the three mixing approaches, finding that the ZSR-style mixing approach takes approximately five to six times longer than aquelec or aquorg. Results are shown in Tables 2.6 and 2.7.

Table 2.6: Time elapsed for multi-run simulations of the AIOMFAC-VISC mixing approaches. Each trial consisted of 200,000 runs. See also Table 2.7.

Trial	aquelec	aquorg	ZSR
1	5.02 s	5.08 s	27.89 s
2	4.39 s	4.38 s	27.45 s
3	4.36 s	4.28 s	23.09 s
4	4.45 s	4.33 s	23.84 s
5	4.33 s	4.33 s	21.66 s

Table 2.7: Mean run time for a test case[a] for each AIOMFAC-VISC mixing approach using a single CPU core[b]. See also Table 2.6.

Trial	aquelec	aquorg	ZSR
1	25.08 µs	25.39 µs	139.45 µs
2	21.95 µs	21.88 µs	137.27 µs
3	21.80 µs	21.41 µs	115.47 µs
4	22.27 µs	21.64 µs	119.22 µs
5	21.64 µs	21.64 µs	108.28 µs

[a] The test case was 1:1 sucrose–$Ca(NO_3)_2$ at $a_w = 0.625$; see Fig. 2.10a.
[b] Processor: Intel(R) Core(TM) i5-6200U CPU @ 2.30GHz

2.7.3 Additional ternary and quaternary aqueous electrolyte mixtures

Figures 2.11 and 2.12 show additional data for ternary and quaternary aqueous electrolyte mixtures.

2.7.4 Cation–anion parameter substitutions

When data is unavailable for certain cation–anion interactions, substitute values are used for the related parameters; see Table 2.8.

Table 2.8: Cation–anion pair substitutions in Table 2.5.

Missing Pair	Replacement Pair
Li^+, Br^-	Li^+, Cl^-
Ca^{2+}, Br^-	Ca^{2+}, Cl^-
Mg^{2+}, Br^-	Mg^{2+}, Cl^-
Ca^{2+}, SO_4^{2-}	Mg^{2+}, SO_4^{2-}
Li^+, HSO_4^-	Na^+, HSO_4^-
K^+, HSO_4^-	Na^+, HSO_4^-
NH_4^+, HSO_4^-	Na^+, HSO_4^-
Ca^{2+}, HSO_4^-	Na^+, HSO_4^-
Mg^{2+}, HSO_4^-	Na^+, HSO_4^-
H^+, I^-	H^+, Br^-
Li^+, I^-	Li^+, Cl^-
NH_4^+, I^-	NH_4^+, Cl^-
Ca^{2+}, I^-	Ca^{2+}, Cl^-
Mg^{2+}, I^-	Mg^{2+}, Cl^-

2.7.5 Scatter among similar measurement points and temperature dependence

The scatter among similar measurement points is one reason for the inclusion of a 2% uncertainty in viscosity applied to all bulk measurements. This is demonstrated by Fig. 2.13, which shows measurements and AIOMFAC-VISC predicted viscosities for temperatures between 268.15 K and 328.15 K.

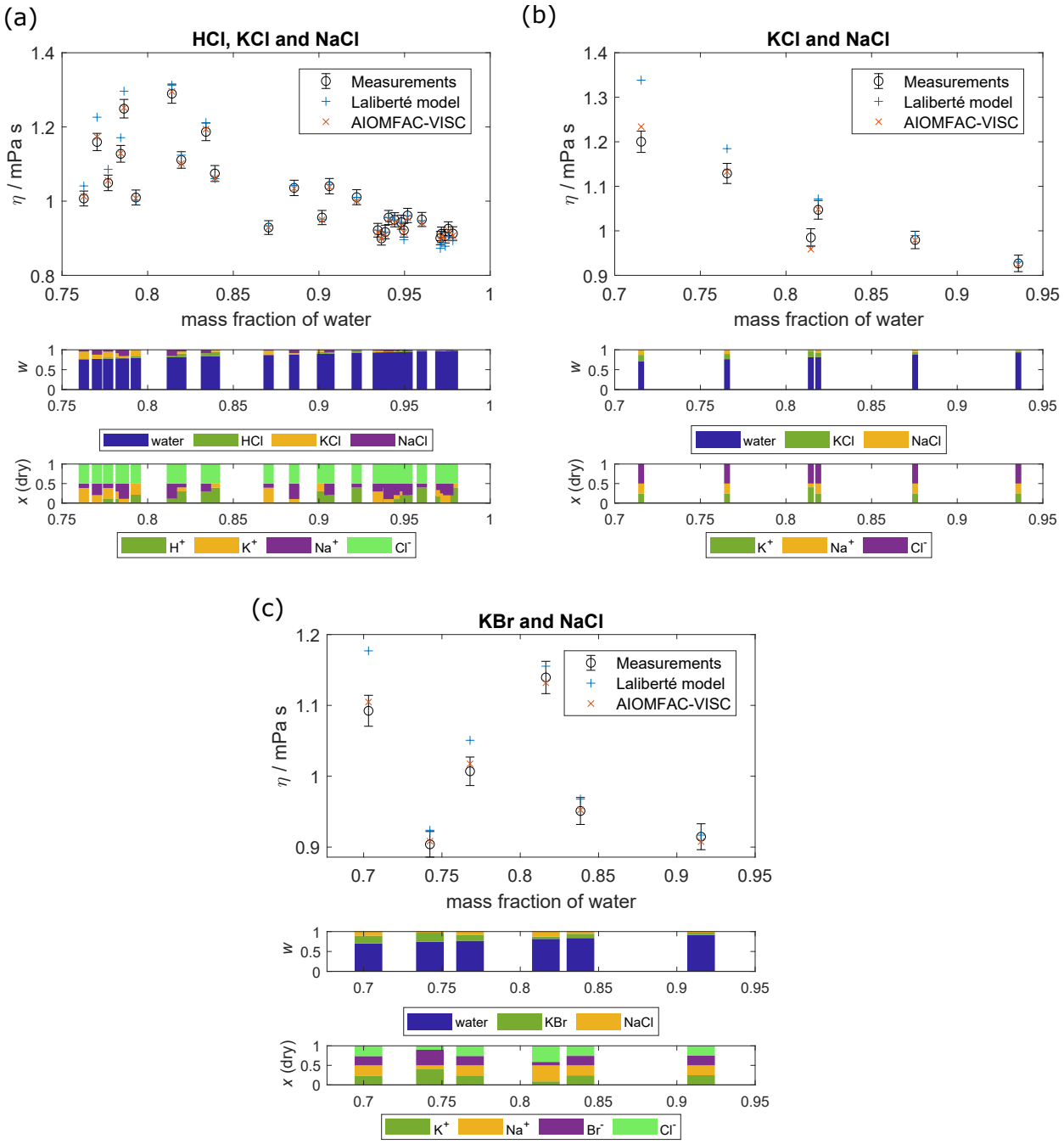

Figure 2.11: Comparison of AIOMFAC-VISC and the Laliberté model for ternary and quaternary aqueous electrolyte mixtures:(a) HCl, KCl, and NaCl; (b) KCl and NaCl; (c) KBr and NaCl. Top panel: viscosity versus mass fraction of water with 2 % error in viscosity included for all measurements. Middle panel: mass fractions of mixture input components. Bottom panel: mole fractions of ions in dry mixture.

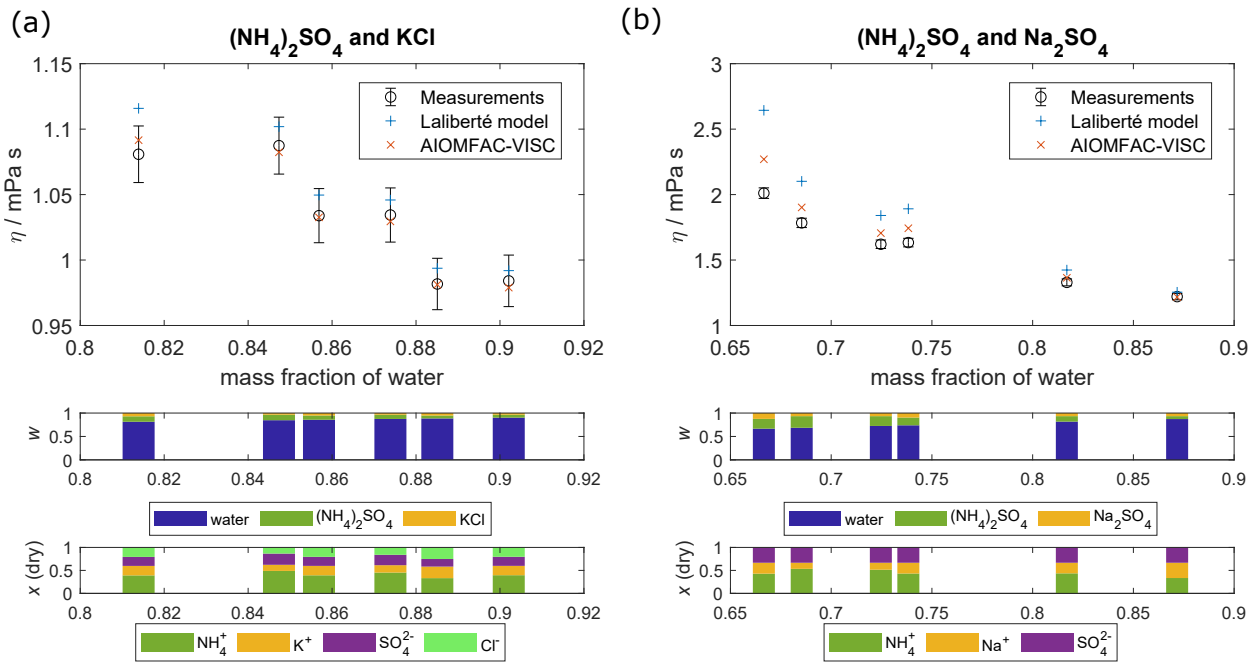

Figure 2.12: Comparison of AIOMFAC-VISC and the Laliberté model for ternary aqueous electrolyte mixtures: (a) $(NH_4)_2SO_4$ and KCl; (b) $(NH_4)_2SO_4$ and Na_2SO_4. Top panel: viscosity versus mass fraction of water with 2 % error in viscosity included for all measurements. Middle panel: mass fractions of mixture input components. Bottom panel: mole fractions of ions in dry mixture.

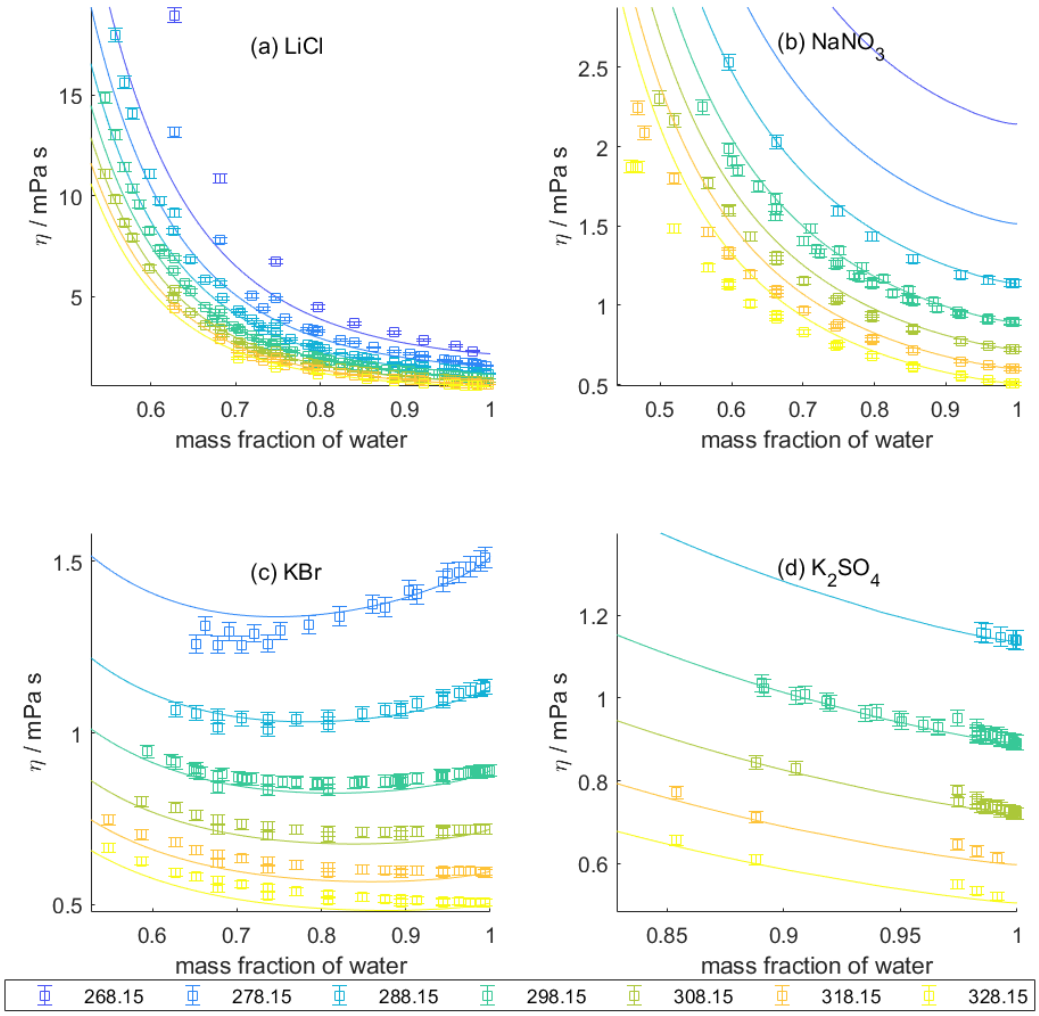

Figure 2.13: Viscosity measurements aggregated by Laliberté (2007a) for a selection of binary aqueous solutions at several temperatures between 268.15 and 323.15 K: (a) LiCl; (b) $NaNO_3$; (c) KBr; (d) K_2SO_4. 2 % viscosity error bars are included to account for scatter among similar measurement points. Solid lines are AIOMFAC-VISC predictions.

Chapter 3

Future Work

3.1 Additional ions and datasets

While AIOMFAC-VISC has been shown to provide excellent viscosity predictions for a wide range of aqueous electrolyte solutions and some organic–inorganic mixtures, it will clearly benefit from the inclusion of additional ions and datasets in future work. AIOMFAC-VISC can currently predict 42 cation–anion interactions, but only 28 of them are fitted to viscosity measurements. The others currently rely on substitute $c_{c,a}$ parameters (see Table 2.8); fitting additional data that contain these cation–anion interactions would be a clear improvement over the current approach. In terms of ions, Yin et al. (in prep.) have recently implemented I^-, IO_3^-, OH^-, and the carbonate–bicarbonate system into AIOMFAC. Viscosity measurements for systems containing these species already exist in accessible form (Laliberté, 2007a), and they could be used to fit even more single-ion and cation–anion parameters for AIOMFAC-VISC. It is expected that most other atmospherically relevant binary aqueous electrolyte solutions will exist primarily as liquids, but there are exceptions. According to Murray et al. (2012), iodic acid, which forms in the marine atmospheric boundary layer from gaseous iodine and organoiodine species, can become highly viscous as an aqueous solution below RH = 10%. We also encourage

further use of droplet-based measurement techniques to determine viscosity of aqueous electrolyte systems for which bulk viscosity measurements already exist; such measurements could be used to further test AIOMFAC-VISC predictions.

Viscosity measurements are most common for binary aqueous electrolyte solutions and they are useful for verification, but atmospheric aerosols are rarely so simple. Additional measurements of ternary and quaternary electrolyte mixtures would provide more realistic analogs to inorganic aerosols and would allow for more detailed comparison of the relative viscosity contributions from dissolved ions and distinct cation–anion pairs. Finally, viscosity measurements for aqueous organic–inorganic mixtures, particularly those containing organic compounds other than sucrose, will be especially valuable. Sucrose is a popular choice for organic–inorganic mixtures because it is well studied and has similar properties to oxygenated compounds in secondary organic aerosol. It also inhibits phase separation in organic–inorganic mixed aerosols, on its own or when added to another organic compound as in Ott et al. (2020). Richards et al. (2020b) explored particle phase state of organic–inorganic mixtures containing the ions Na^{+}, Ca^{2+}, Mg^{2+}, and SO_4^{2-}, and oxygenated organic compounds with molecular weights below 310 Da including glucose, gluconic acid, glucuronic acid, N-acetylneuraminic acid, and sorbitol. While viscosity data are shown in their figures, tabulated data were not yet available during the preparation of this thesis. In the future, we plan to obtain and examine these data, as they present an excellent opportunity to further test the three mixing approaches that were developed.

3.2 Diffusion and phase separation

Diffusion coefficients are essential to understanding aerosol processes in dynamic meteorological simulations and kinetic process models of outdoor and indoor aerosols, because they can be used to calculate the timescale of heterogeneous chemistry, simulate dynamic

gas–particle partitioning, and study hygroscopic growth (Shiraiwa et al., 2011, 2013; Zhou et al., 2019; Huang et al., 2021). One of the primary methods of calculating diffusion coefficients is the Stokes–Einstein relation,

$$D_j = \frac{k_{\mathrm{B}} T}{6\pi\eta R_j}, \tag{3.1}$$

where D_j is the diffusion coefficient and R_j is the effective molecular radius for diffusing species j, k_{B} is the Boltzmann constant, and η is the mixture viscosity. The Stokes–Einstein relation has proven effective at estimating diffusion coefficients of organic compounds in organic–water mixtures, but breaks down when the radius of the diffusing species is much smaller than the radius of the species that make up the molecular matrix, which makes the diffusion of water molecules difficult to determine (Evoy et al., 2019). A fractional Stokes–Einstein relation has been shown to work well in this case, and can be expressed as

$$\frac{D}{D_{\mathrm{w}}} = \left(\frac{\eta_{\mathrm{w}}}{\eta}\right)^{\zeta}, \tag{3.2}$$

where D_{w} is the measured diffusion coefficient for pure water at given temperature and ζ is an adjustable parameter. Evoy et al. (2020) demonstrated that a fitted version of this equation, where ζ is a monotonic function of R_{diff} (R_j) and R_{matrix}, could accurately predict 135 out of 138 diffusion coefficient measurements – 98 % – to within a factor of 10. It remains to be seen if this equation would also accommodate the estimation of diffusivities in aqueous organic–inorganic mixtures.

As mentioned in Chapter 2, thermodynamics can favor liquid–liquid phase separation or solid–liquid phase separation in aerosol particles (Zuend et al., 2010). In liquid–liquid phase-separated aerosol, a common arrangement is a core–shell morphology, comprising an organic-rich shell and an aqueous inorganic-rich core (Stewart et al., 2015; Gorkowski et al., 2020). As mixtures containing oxygenated secondary organic aerosol

components tend to be more viscous than aqueous electrolyte solutions, the diffusion coefficients of components within the organic-rich shell will generally be of greater interest for characterizing dynamic processes. In such cases, deliquescence and efflorescence of the electrolyte-rich core may be rate limited by water diffusion through the organic shell, especially if the shell is highly viscous. Some ions will be partially soluble in the organic-rich phase, and their influence must also be considered. Ions are hygroscopic, and their presence will draw more water into the organic-rich phase, lowering its viscosity with water acting as a plasticizer. This effect could have a substantial impact on the viscosity of the organic-rich phase, so AIOMFAC-VISC predictions are highly dependent on the accuracy of the liquid–liquid phase separation model. If the organic shell is not viscous, diffusion is not expected to be the determining factor for heterogeneous chemistry. In fact, heterogeneous oxidation (of organic compounds) can actually increase in a phase-separated aerosol because the concentration of organic species increases at the surface relative to the concentration in a single-phase particle (Lam et al., 2021).

Huang et al. (2021) observed three coexisting liquid phases in aerosol surrogate mixtures consisting of primary organic aerosol, secondary organic aerosol, and secondary inorganic aerosol. The polarity spread of the organic species plays a large role in determining the number of liquid phases: these authors found that when the average oxygen-to-carbon ratio of the SOA species is below 0.8, three liquid phases form and when it is above 0.8, three phases do not form. For liquid–liquid phase-separated aerosols, separate viscosity calculations must be completed for each phase. Using our viscosity prediction framework, AIOMFAC must first calculate liquid–liquid equilibrium, which is by far the most computationally expensive part (Zuend et al., 2010). This means the time spent on viscosity calculation, whether by the single-run aquelec or the iterative ZSR mixing rule, will be comparatively small.

3.3 Gel transitions

Some aerosol droplets containing certain ions can undergo a gel transition. Unlike smooth increases in viscosity, gel transitions tend to happen abruptly when RH decreases and crosses a relatively narrow threshold in RH. When this occurs, hydrated cation–anion pairs form chains that create a rigid structure. For example, Cai et al. (2015) observed an abrupt transition from fast water loss to slow water release for aqueous $\mathrm{MgSO_4}$ droplets as RH was decreased below 40 %. They also reported apparent diffusion coefficients for water in the aqueous $\mathrm{MgSO_4}$ gel, finding that diffusion is severely reduced but not to the same degree as is observed in glassy aerosol. This is due to observed inhomogeneities in the gel surface (Sjogren et al., 2007) and a sponge-like interior that allows free water molecules to diffuse between the bulk and the surface. Davies and Wilson (2016) found similar results for aqueous $\mathrm{MgSO_4}$.

More recently, Richards et al. (2020b) suggested that ion–organic interactions could play an important role in gel formation for organic–inorganic mixtures. According to their hypothesis, divalent ions form complexes with organic molecules which form an interlocking structure when water content is sufficiently reduced, i.e., at equilibrium with a low RH. Organic–inorganic mixtures containing divalent ions like $\mathrm{Ca^{2+}}$, $\mathrm{Mg^{2+}}$, and $\mathrm{SO_4^{2-}}$ underwent gel transition, whereas mixtures containing NaCl did not. Song et al. (2021) considered the potential formation of gels in the systems shown in Fig. 2.10, but were not able to make that determination.

A strength of AIOMFAC is that it explicitly captures ion–organic interactions within its activity coefficients. AIOMFAC-VISC's use of ion activities in its equation for molar Gibbs energy for viscous flow implies that these ion–organic interactions are represented in viscosity calculations, albeit indirectly. However, the current version of AIOMFAC-VISC does not predict a gel transition for any systems. AIOMFAC-VISC includes a cation–anion contribution to molar Gibbs energy for viscous flow. It is possible that this term

could be modified to represent non-Newtonian gels in a Newtonian fashion, e.g., assigning a stepwise contribution that activates for certain cation–anion pairs or perhaps all cation–anion pairs that include a divalent ion. For this approach to work, gels must be represented by a sufficiently large viscosity value. In Richards et al. (2020b), a value close to $10^{10}\ \mathrm{Pa\,s}$ was used, but the lower error bars sometimes extended below $10^{8}\ \mathrm{Pa\,s}$, and no upper viscosity limit has been proposed or well characterized.

3.4 Closing remarks

Aerosol viscosity is an interdisciplinary research problem, drawing on knowledge from several fields including atmospheric science, chemistry, and materials science. Earlier literature on viscosity models, particularly studies on the Jones–Dole and Eyring frameworks, were essential in the creation of our model for aqueous electrolyte solutions. The scarcity of viscosity measurements for aqueous electrolyte mixtures and aqueous organic–inorganic mixtures presented a challenge in fitting the model. Developing a predictive viscosity model for aerosol particles could have taken multiple routes, as evidenced by the three mixing approaches we described to combine our electrolyte model with the organic model from Gervasi et al. (2020). The AIOMFAC framework (Zuend et al., 2008, 2011) is already widely used in aerosol studies, and the updated AIOMFAC-VISC model will soon be available for use at https://aiomfac.lab.mcgill.ca/model.html.

We hope that future work on diffusion modeling, phase separation, gel formation, and other aspects of aerosol phase state will benefit from the existence of our predictive viscosity model for aerosols, enabling further research and understanding of the role of aerosols in the atmosphere.

Bibliography

Abdulagatov, I. M., Zeinalova, A. A., and Azizov, N. D. (2004). Viscosity of the Aqueous Ca(NO $_3$) $_2$ Solutions at Temperatures from 298 to 573 K and at Pressures up to 40 MPa. *Journal of Chemical & Engineering Data*, 49(5):1444–1450.

Abrams, D. S. and Prausnitz, J. M. (1975). Statistical thermodynamics of liquid mixtures: A new expression for the excess Gibbs energy of partly or completely miscible systems. *AIChE Journal*, 21(1):116–128. _eprint: https://aiche.onlinelibrary.wiley.com/doi/pdf/10.1002/aic.690210115.

Ariya, P. A., Amyot, M., Dastoor, A., Deeds, D., Feinberg, A., Kos, G., Poulain, A., Ryjkov, A., Semeniuk, K., Subir, M., and Toyota, K. (2015). Mercury Physicochemical and Biogeochemical Transformation in the Atmosphere and at Atmospheric Interfaces: A Review and Future Directions. *Chemical Reviews*, 115(10):3760–3802.

Bajić, D. M., Šerbanović, S. P., Živković, E. M., Jovanović, J., and Kijevčanin, M. L. (2014). Prediction and correlation of viscosity of binary mixtures of ionic liquids with organic solvents. *Journal of Molecular Liquids*, 197:1–6.

Baldelli, A., Power, R. M., Miles, R. E. H., Reid, J. P., and Vehring, R. (2016). Effect of crystallization kinetics on the properties of spray dried microparticles. *Aerosol Science and Technology*, 50(7):693–704.

Bateman, A. P., Bertram, A. K., and Martin, S. T. (2015). Hygroscopic Influence on the Semisolid-to-Liquid Transition of Secondary Organic Materials. *The Journal of Physical Chemistry A*, 119(19):4386–4395.

Bateman, A. P., Gong, Z., Liu, P., Sato, B., Cirino, G., Zhang, Y., Artaxo, P., Bertram, A. K., Manzi, A. O., Rizzo, L. V., Souza, R. A. F., Zaveri, R. A., and Martin, S. T. (2016). Sub-micrometre particulate matter is primarily in liquid form over Amazon rainforest. *Nature Geoscience*, 9(1):34–37. Number: 1 Publisher: Nature Publishing Group.

Boender, C. G. E., Rinnooy Kan, A. H. G., Timmer, G. T., and Stougie, L. (1982). A stochastic method for global optimization. *Mathematical Programming*, 22(1):125–140.

Cai, C., Tan, S., Chen, H., Ma, J., Wang, Y., P. Reid, J., and Zhang, Y. (2015). Slow water transport in MgSO 4 aerosol droplets at gel-forming relative humidities. *Physical Chemistry Chemical Physics*, 17(44):29753–29763.

Cox, W. M., Wolfenden, J. H., and Hartley, H. B. (1934). The viscosity of strong electrolytes measured by a differential method. *Proceedings of the Royal Society of London. Series A, Containing Papers of a Mathematical and Physical Character*, 145(855):475–488.

Csendes, T. (1988). Nonlinear parameter estimation by global optimization-efficiency and reliability. *Acta Cybernetica*, 8(4):361–370.

Davies, J. F. and Wilson, K. R. (2016). Raman Spectroscopy of Isotopic Water Diffusion in Ultraviscous, Glassy, and Gel States in Aerosol by Use of Optical Tweezers. *Analytical Chemistry*, 88(4):2361–2366.

Dehaoui, A., Issenmann, B., and Caupin, F. (2015). Viscosity of deeply supercooled water and its coupling to molecular diffusion. *Proceedings of the National Academy of Sciences*, 112(39):12020–12025.

DeRieux, W.-S. W., Li, Y., Lin, P., Laskin, J., Laskin, A., Bertram, A. K., Nizkorodov, S. A., and Shiraiwa, M. (2018). Predicting the glass transition temperature and viscosity of

secondary organic material using molecular composition. *Atmospheric Chemistry and Physics*, 18(9):6331–6351.

Esteves, M. J. C., Cardoso, M. J. E. d. M., and Barcia, O. E. (2001). A Debye–Hückel Model for Calculating the Viscosity of Binary Strong Electrolyte Solutions. *Industrial & Engineering Chemistry Research*, 40(22):5021–5028.

Evoy, E., Kamal, S., Patey, G. N., Martin, S. T., and Bertram, A. K. (2020). Unified Description of Diffusion Coefficients from Small to Large Molecules in Organic–Water Mixtures. *The Journal of Physical Chemistry A*, 124(11):2301–2308.

Evoy, E., Maclean, A. M., Rovelli, G., Li, Y., Tsimpidi, A. P., Karydis, V. A., Kamal, S., Lelieveld, J., Shiraiwa, M., Reid, J. P., and Bertram, A. K. (2019). Predictions of diffusion rates of large organic molecules in secondary organic aerosols using the Stokes–Einstein and fractional Stokes–Einstein relations. *Atmospheric Chemistry and Physics*, 19(15):10073–10085.

Fard, M. M., Krieger, U. K., and Peter, T. (2017). Kinetic Limitation to Inorganic Ion Diffusivity and to Coalescence of Inorganic Inclusions in Viscous Liquid–Liquid Phase-Separated Particles. *The Journal of Physical Chemistry A*, 121(48):9284–9296.

Fredenslund, A., Jones, R. L., and Prausnitz, J. M. (1975). Group-contribution estimation of activity coefficients in nonideal liquid mixtures. *AIChE Journal*, 21(6):1086–1099. _eprint: https://aiche.onlinelibrary.wiley.com/doi/pdf/10.1002/aic.690210607.

Fu, H., Zhang, M., Li, W., Chen, J., Wang, L., Quan, X., and Wang, W. (2012). Morphology, composition and mixing state of individual carbonaceous aerosol in urban Shanghai. *Atmospheric Chemistry and Physics*, 12(2):693–707.

Gervasi, N. R., Topping, D. O., and Zuend, A. (2020). A predictive group-contribution model for the viscosity of aqueous organic aerosol. *Atmospheric Chemistry and Physics*, 20(5):2987–3008.

Glasstone, S., Laidler, K., and Eyring, H. (1941). *The theory of rate processes: the kinetics of chemical reactions, viscosity, diffusion and electrochemical phenomena*. McGraw-Hill, 1st ed. edition.

Goldsack, D. E. and Franchetto, A. A. (1977a). The viscosity of concentrated electrolyte solutions—III. A mixture law. *Electrochimica Acta*, 22(11):1287–1294.

Goldsack, D. E. and Franchetto, R. (1977b). The viscosity of concentrated electrolyte solutions. I. Concentration dependence at fixed temperature. *Canadian Journal of Chemistry*, 55(6):1062–1072.

Goldsack, D. E. and Franchetto, R. C. (1978). The viscosity of concentrated electrolyte solutions. II. Temperature dependence. *Canadian Journal of Chemistry*, 56(10):1442–1450.

Gorkowski, K., Donahue, N. M., and Sullivan, R. C. (2020). Aerosol Optical Tweezers Constrain the Morphology Evolution of Liquid-Liquid Phase-Separated Atmospheric Particles. *Chem*, 6(1):204–220.

Hallquist, M., Wenger, J. C., Baltensperger, U., Rudich, Y., Simpson, D., Claeys, M., Dommen, J., Donahue, N. M., George, C., Goldstein, A. H., Hamilton, J. F., Herrmann, H., Hoffmann, T., Iinuma, Y., Jang, M., Jenkin, M. E., Jimenez, J. L., Kiendler-Scharr, A., Maenhaut, W., McFiggans, G., Mentel, T. F., Monod, A., Prévôt, A. S. H., Seinfeld, J. H., Surratt, J. D., Szmigielski, R., and Wildt, J. (2009). The formation, properties and impact of secondary organic aerosol: current and emerging issues. *Atmospheric Chemistry and Physics*, 9(14):5155–5236.

Heald, C. L. and Kroll, J. H. (2020). The fuel of atmospheric chemistry: Toward a complete description of reactive organic carbon. *Science Advances*, 6(6):eaay8967.

Hu, Y.-F. and Lee, H. (2003). Prediction of viscosity of mixed electrolyte solutions based on the Eyring's absolute rate theory and the semi-ideal hydration model. *Electrochimica Acta*, 48(13):1789–1796.

Huang, Y., Mahrt, F., Xu, S., Shiraiwa, M., Zuend, A., and Bertram, A. K. (2021). Coexistence of three liquid phases in individual atmospheric aerosol particles. *Proceedings of the National Academy of Sciences*, 118(16). ISBN: 9782102512117 Publisher: National Academy of Sciences Section: Physical Sciences.

Irving, J. B. (1977). *Viscosities of binary liquid mixtures :the effectiveness of mixture equations /*. East Kilbride, Scotland :.

Jenkins, H. D. B. and Marcus, Y. (1995). Viscosity B-Coefficients of Ions in Solution. *Chemical Reviews*, 95(8):2695–2724.

Jones, G. and Dole, M. (1929). The viscosity of aqueous solutions of strong electrolytes with special reference to barium chloride. *Journal of the American Chemical Society*, 51(10):2950–2964.

Kaminsky, M. (1957). Untersuchungen über die Wechselwirkung Ion-Lösungsmittel, insbesondere auf Grund von Viskositätsmessungen. *Zeitschrift für Naturforschung A*, 12(5):424–433. Publisher: Verlag der Zeitschrift für Naturforschung Section: Zeitschrift für Naturforschung A.

Kiriukhin, M. Y. and Collins, K. D. (2002). Dynamic hydration numbers for biologically important ions. *Biophysical Chemistry*, 99(2):155–168.

Kohanski, M. A., Lo, L. J., and Waring, M. S. (2020). Review of indoor aerosol generation, transport, and control in the context of COVID-19. *International Forum of Allergy & Rhinology*, 10(10):1173–1179. _eprint: https://onlinelibrary.wiley.com/doi/pdf/10.1002/alr.22661.

Koop, T., Bookhold, J., Shiraiwa, M., and Pöschl, U. (2011). Glass transition and phase state of organic compounds: dependency on molecular properties and implications for secondary organic aerosols in the atmosphere. *Physical Chemistry Chemical Physics*, 13(43):19238–19255.

Laliberté, M. (2007a). Model for Calculating the Viscosity of Aqueous Solutions. *Journal of Chemical & Engineering Data*, 52(2):321–335.

Laliberté, M. (2007b). Model for Calculating the Viscosity of Aqueous Solutions,. *Journal of Chemical & Engineering Data*, 52(4):1507–1508.

Laliberté, M. (2009). A Model for Calculating the Heat Capacity of Aqueous Solutions, with Updated Density and Viscosity Data. *Journal of Chemical & Engineering Data*, 54(6):1725–1760.

Lam, H. K., Xu, R., Choczynski, J., Davies, J. F., Ham, D., Song, M., Zuend, A., Li, W., Tse, Y.-L. S., and Chan, M. N. (2021). Effects of liquid–liquid phase separation and relative humidity on the heterogeneous OH oxidation of inorganic–organic aerosols: insights from methylglutaric acid and ammonium sulfate particles. *Atmospheric Chemistry and Physics*, 21(3):2053–2066.

Lencka, M. M., Anderko, A., Sanders, S. J., and Young, R. D. (1998). Modeling Viscosity of Multicomponent Electrolyte Solutions. *International Journal of Thermophysics*, 19(2):367–378.

Li, Y.-J., Liu, P.-F., Bergoend, C., Bateman, A. P., and Martin, S. T. (2017). Rebounding hygroscopic inorganic aerosol particles: Liquids, gels, and hydrates. *Aerosol Science and Technology*, 51(3):388–396.

Marcus, Y. (2009). Effect of ions on the structure of water: structure making and breaking. *Chemical reviews*, 109(3):1346–1370.

Miller, A. (2003). Global optimization using the Boender-Timmer-Rinnoy Kan algorithm. https://www.mat.univie.ac.at/ neum/glopt/contrib/global.f90.

Moré, J. J., Garbow, B. S., and Hillstrom, K. E. (1980). User guide for MINPACK-1. Technical report, CM-P00068642.

Moré, J. J., Sorensen, D. C., Hillstrom, K., and Garbow, B. (1984). The MINPACK project. *Sources and development of mathematical software*, 25:88–111.

Murray, B. J., Haddrell, A. E., Peppe, S., Davies, J. F., Reid, J. P., O'Sullivan, D., Price, H. C., Kumar, R., Saunders, R. W., Plane, J. M. C., Umo, N. S., and Wilson, T. W. (2012). Glass formation and unusual hygroscopic growth of iodic acid solution droplets with relevance for iodine mediated particle formation in the marine boundary layer. *Atmospheric Chemistry and Physics*, 12(18):8575–8587.

Nowlan, M.-F., Doan, T. H., and Sangster, J. (1980). Prediction of the viscosity of mixed electrolyte solutions from single-salt data. *The Canadian Journal of Chemical Engineering*, 58(5):637–642. _eprint: https://onlinelibrary.wiley.com/doi/pdf/10.1002/cjce.5450580514.

Ott, E.-J. E., Tackman, E. C., and Freedman, M. A. (2020). Effects of Sucrose on Phase Transitions of Organic/Inorganic Aerosols. *ACS Earth and Space Chemistry*, 4(4):591–601.

Pilinis, C., Pandis, S. N., and Seinfeld, J. H. (1995). Sensitivity of direct climate forcing by atmospheric aerosols to aerosol size and composition. *Journal of Geophysical Research: Atmospheres*, 100(D9):18739–18754. _eprint: https://agupubs.onlinelibrary.wiley.com/doi/pdf/10.1029/95JD02119.

Power, R., Simpson, S., Reid, J., and Hudson, A. (2013). The transition from liquid to solid-like behaviour in ultrahigh viscosity aerosol particles. *Chemical Science*, 4(6):2597–2604.

Pye, H. O. T., Nenes, A., Alexander, B., Ault, A. P., Barth, M. C., Clegg, S. L., Collett Jr., J. L., Fahey, K. M., Hennigan, C. J., Herrmann, H., Kanakidou, M., Kelly, J. T., Ku, I.-T., McNeill, V. F., Riemer, N., Schaefer, T., Shi, G., Tilgner, A., Walker, J. T., Wang, T., Weber, R., Xing, J., Zaveri, R. A., and Zuend, A. (2020). The acidity of atmospheric particles and clouds. *Atmospheric Chemistry and Physics*, 20(8):4809–4888.

Pye, H. O. T., Zuend, A., Fry, J. L., Isaacman-VanWertz, G., Capps, S. L., Appel, K. W., Foroutan, H., Xu, L., Ng, N. L., and Goldstein, A. H. (2018). Coupling of organic and inorganic aerosol systems and the effect on gas–particle partitioning in the southeastern US. *Atmospheric Chemistry and Physics*, 18(1):357–370.

Rafferty, A. and Preston, T. C. (2018). Measuring the size and complex refractive index of an aqueous aerosol particle using electromagnetic heating and cavity-enhanced Raman scattering. *Physical Chemistry Chemical Physics*, 20(25):17038–17047.

Reid, J. P., Bertram, A. K., Topping, D. O., Laskin, A., Martin, S. T., Petters, M. D., Pope, F. D., and Rovelli, G. (2018). The viscosity of atmospherically relevant organic particles. *Nature Communications*, 9(1):956.

Renbaum-Wolff, L., Grayson, J. W., Bateman, A. P., Kuwata, M., Sellier, M., Murray, B. J., Shilling, J. E., Martin, S. T., and Bertram, A. K. (2013). Viscosity of α-pinene secondary organic material and implications for particle growth and reactivity. *Proceedings of the National Academy of Sciences*, 110(20):8014–8019. Publisher: National Academy of Sciences Section: Physical Sciences.

Richards, D. S., Trobaugh, K. L., Hajek-Herrera, J., and Davis, R. D. (2020a). Dual-Balance Electrodynamic Trap as a Microanalytical Tool for Identifying Gel Transitions and Viscous Properties of Levitated Aerosol Particles. *Analytical Chemistry*, 92(4):3086–3094.

Richards, D. S., Trobaugh, K. L., Hajek-Herrera, J., Price, C. L., Sheldon, C. S., Davies, J. F., and Davis, R. D. (2020b). Ion-molecule interactions enable unexpected phase transitions in organic-inorganic aerosol. *Science Advances*, 6(47):eabb5643.

Rothfuss, N. E. and Petters, M. D. (2017). Characterization of the temperature and humidity-dependent phase diagram of amorphous nanoscale organic aerosols. *Physical Chemistry Chemical Physics*, 19(9):6532–6545.

Rovelli, G., Song, Y.-C., Maclean, A. M., Topping, D. O., Bertram, A. K., and Reid, J. P. (2019). Comparison of Approaches for Measuring and Predicting the Viscosity of Ternary Component Aerosol Particles. *Anal. Chem.*, page 9.

Roy, M. N., Jha, A., and Choudhury, A. (2004). Densities, Viscosities and Adiabatic Compressibilities of Some Mineral Salts in Water at Different Temperatures. *Journal of Chemical & Engineering Data*, 49(2):291–296.

Seinfeld, J. H. and Pandis, S. N. (2016). *Atmospheric Chemistry and Physics: From Air Pollution to Climate Change*. John Wiley & Sons, Incorporated, New York, UNITED STATES.

Shannon, R. D. (1976). Revised Effective Ionic Radii and Systematic Studies of Interatomic Distances in Halides and Chaleogenides. *Acta Crystallogr., Sect. A*, 32(5):751–767.

Shiraiwa, M., Ammann, M., Koop, T., and Pöschl, U. (2011). Gas uptake and chemical aging of semisolid organic aerosol particles. *Proceedings of the National Academy of Sciences*, 108(27):11003–11008.

Shiraiwa, M. and Seinfeld, J. H. (2012). Equilibration timescale of atmospheric secondary organic aerosol partitioning. *Geophysical Research Letters*, 39(24). _eprint: https://agupubs.onlinelibrary.wiley.com/doi/pdf/10.1029/2012GL054008.

Shiraiwa, M., Zuend, A., Bertram, A. K., and Seinfeld, J. H. (2013). Gas–particle partitioning of atmospheric aerosols: interplay of physical state, non-ideal mixing and morphology. *Physical Chemistry Chemical Physics*, 15(27):11441.

Sjogren, S., Gysel, M., Weingartner, E., Baltensperger, U., Cubison, M. J., Coe, H., Zardini, A. A., Marcolli, C., Krieger, U. K., and Peter, T. (2007). Hygroscopic growth and water uptake kinetics of two-phase aerosol particles consisting of ammonium sulfate, adipic and humic acid mixtures. *Journal of Aerosol Science*, 38(2):157–171.

Song, Y.-C., Lilek, J., Lee, J. B., Chan, M. N., Wu, Z., Zuend, A., and Song, M. (2021). Viscosity and phase state of aerosol particles consisting of sucrose mixed with inorganic salts. *Atmospheric Chemistry and Physics Discussions*, pages 1–32.

Stewart, D. J., Cai, C., Nayler, J., Preston, T. C., Reid, J. P., Krieger, U. K., Marcolli, C., and Zhang, Y. H. (2015). Liquid–Liquid Phase Separation in Mixed Organic/Inorganic Single Aqueous Aerosol Droplets. *The Journal of Physical Chemistry A*, 119(18):4177–4190.

Stokes, R. H. and Robinson, R. A. (1966). Interactions in aqueous nonelectrolyte solutions .i. Solute-solvent equilibria. *J. Phys. Chem.*, 70(7):2126–2130.

Storn, R. and Price, K. (1997). Differential Evolution – A Simple and Efficient Heuristic for global Optimization over Continuous Spaces. *Journal of Global Optimization*, 11(4):341–359.

Tan, I., Storelvmo, T., and Choi, Y.-S. (2014). Spaceborne lidar observations of the ice-nucleating potential of dust, polluted dust, and smoke aerosols in mixed-phase clouds. *Journal of Geophysical Research: Atmospheres*, 119(11):6653–6665. _eprint: https://agupubs.onlinelibrary.wiley.com/doi/pdf/10.1002/2013JD021333.

Virtanen, A., Joutsensaari, J., Koop, T., Kannosto, J., Yli-Pirilä, P., Leskinen, J., Mäkelä, J. M., Holopainen, J. K., Pöschl, U., Kulmala, M., Worsnop, D. R., and Laaksonen, A. (2010). An amorphous solid state of biogenic secondary organic aerosol particles. *Nature*, 467(7317):824–827.

Viswanath, D. S., Ghosh, T. K., Prasad, D. H. L., Dutt, N. V. K., and Rani, K. Y. (2007). *Viscosity of Liquids: Theory, Estimation, Experiment, and Data*. Springer Science & Business Media.

Wahab, A. and Mahiuddin, S. (2001). Isentropic Compressibility and Viscosity of Aqueous and Methanolic Calcium Chloride Solutions. *Journal of Chemical & Engineering Data*, 46(6):1457–1463.

Wallace, B. J. and Preston, T. C. (2019). Water Uptake and Loss in Viscous Aerosol Particles with Concentration-Dependent Diffusivities. *The Journal of Physical Chemistry A*, 123(15):3374–3382.

Wang, P., Anderko, A., and Young, R. D. (2004). Modeling viscosity of concentrated and mixed-solvent electrolyte systems. *Fluid Phase Equilibria*, 226:71–82.

Yau, M. K. and Rogers, R. R. (1996). *A short course in cloud physics*. Elsevier.

Zdanovskii, A. B. (1936). Untitled. *Tr. Solyanoi Lab. Akad. Nauk SSSR*, (6):5–70.

Zdanovskii, A. B. (1948). New methods of calculating solubilities of electrolytes in multicomponent systems. *Zh. Fiz. Khim.*, 22(12):1478–1485.

Zhang and Han (1996). Viscosity and Density of Water + Sodium Chloride + Potassium Chloride Solutions at 298.15 K. *Journal of Chemical & Engineering Data*, 41(3):516–520.

Zhang, Q., Jimenez, J. L., Canagaratna, M. R., Allan, J. D., Coe, H., Ulbrich, I., Alfarra, M. R., Takami, A., Middlebrook, A. M., Sun, Y. L., Dzepina, K., Dunlea, E., Docherty, K., DeCarlo, P. F., Salcedo, D., Onasch, T., Jayne, J. T., Miyoshi, T., Shimono, A., Hatakeyama, S., Takegawa, N., Kondo, Y., Schneider, J., Drewnick, F., Borrmann, S., Weimer, S., Demerjian, K., Williams, P., Bower, K., Bahreini, R., Cottrell, L., Griffin, R. J., Rautiainen, J., Sun, J. Y., Zhang, Y. M., and Worsnop, D. R. (2007). Ubiquity and dominance of oxygenated species in organic aerosols in anthropogenically-influenced Northern Hemisphere midlatitudes. *Geophysical Research Letters*, 34(13). _eprint: https://agupubs.onlinelibrary.wiley.com/doi/pdf/10.1029/2007GL029979.

Zhou, S., Hwang, B. C. H., Lakey, P. S. J., Zuend, A., Abbatt, J. P. D., and Shiraiwa, M. (2019). Multiphase reactivity of polycyclic aromatic hydrocarbons is driven by phase separation and diffusion limitations. *Proceedings of the National Academy of Sciences*, 116(24):11658–11663. Publisher: National Academy of Sciences Section: Physical Sciences.

Zobrist, B., Marcolli, C., Pedernera, D. A., and Koop, T. (2008). Do atmospheric aerosols form glasses? *Atmos. Chem. Phys.*, page 24.

Zuend, A., Marcolli, C., Booth, A. M., Lienhard, D. M., Soonsin, V., Krieger, U. K., Topping, D. O., McFiggans, G., Peter, T., and Seinfeld, J. H. (2011). New and extended parameterization of the thermodynamic model AIOMFAC: calculation of activity coefficients for organic-inorganic mixtures containing carboxyl, hydroxyl, carbonyl, ether, ester, alkenyl, alkyl, and aromatic functional groups. *Atmospheric Chemistry and Physics*, 11(17):9155–9206.

Zuend, A., Marcolli, C., Luo, B. P., and Peter, T. (2008). A thermodynamic model of mixed organic-inorganic aerosols to predict activity coefficients. *Atmos. Chem. Phys.*, page 35.

Zuend, A., Marcolli, C., Peter, T., and Seinfeld, J. H. (2010). Computation of liquid-liquid equilibria and phase stabilities: implications for RH-dependent gas/particle partitioning of organic-inorganic aerosols. *Atmospheric Chemistry and Physics*, 10(16):7795–7820.

Zuend, A. and Seinfeld, J. H. (2012). Modeling the gas-particle partitioning of secondary organic aerosol: the importance of liquid-liquid phase separation. *Atmospheric Chemistry and Physics*, 12(9):3857–3882.